SINGLE AXIS PRECISE MOTION CONTROL USING PIEZOACTUATOR ASSOCIATED WITH A COMPLIANT MECHANISM

A THESIS SUBMITTED TO
THE GRADUATE SCHOOL OF NATURAL AND APPLIED SCIENCES
OF
MIDDLE EAST TECHNICAL UNIVERSITY

BY

GÖKHAN YAŞAR

IN PARTIAL FULFILLMENT OF THE REQUIREMENTS
FOR
THE DEGREE OF MASTER OF SCIENCE
IN
MECHANICAL ENGINEERING

SEPTEMBER 2013

Approval of the thesis:

SINGLE AXIS PRECISE MOTION CONTROL USING PIEZOACTUATOR ASSOCIATED WITH A COMPLIANT MECHANISM

submitted by **GÖKHAN YAŞAR** in partial fulfillment of the requirements for the degree of **Master of Science in Mechanical Engineering Department, Middle East Technical University** by,

Prof. Dr. Canan Özgen
Dean, Graduate School of **Natural and Applied Sciences** ________________

Prof. Dr. Süha Oral
Head of Department, **Mechanical Engineering** ________________

Prof. Dr. Tuna Balkan
Supervisor, **Mechanical Engineering Dept., METU** ________________

Prof. Dr. Yavuz Yaman
Co-supervisor, **Aerospace Engineering Dept., METU** ________________

Examining Committee Members:

Prof. Dr. Y. Samim Ünlüsoy
Mechanical Engineering Department, METU ________________

Prof. Dr. Tuna Balkan
Mechanical Engineering Department, METU ________________

Prof. Dr. Yavuz Yaman
Aerospace Engineering Department, METU ________________

Assist. Prof. Dr. Buğra Koku
Mechanical Engineering Department, METU ________________

Assist. Prof. Dr. Kıvanç Azgın
Mechanical Engineering Department, METU ________________

Date: 03.09.2013

I hereby declare that all information in this document has been obtained and presented in accordance with academic rules and ethical conduct. I also declare that, as required by these rules and conduct, I have fully cited and referenced all material and results that are not original to this work.

Name, Last Name: GÖKHAN YAŞAR

Signature :

ABSTRACT

SINGLE AXIS PRECISE MOTION CONTROL USING PIEZOACTUATOR ASSOCIATED WITH A COMPLIANT MECHANISM

YAŞAR, Gökhan
M.S., Department of Mechanical Engineering
Supervisor : Prof. Dr. Tuna Balkan
Co-Supervisor : Prof. Dr. Yavuz Yaman

September 2013, 72 pages

In this study, 1-D motion control of a moving stage is implemented using a Piezo-stack actuator. Mechanical amplification is achieved using a multi-flexure-hinge based compliant mechanism, due to limited displacement range of piezoactuator. In the design stage of mechanism, a comparison matrix analysis is performed to decide the best alternative among the possible compliant mechanism candidates.

The mechanical design parameters of the displacement amplifier is determined optimally using the analytical equation derived using Pseudo Rigid Body Model, and the static analysis is performed using finite element method to validate the analytical findings. The control system is implemented both to compensate the hysteresis effect and procure precise positioning. In this manner, a model based feedforward model (Bouc-Wen Model) is used as hysteresis compensation and a Proportional Integral (PI) control is used to minimize the error between the desired and actual position. In addition, Zero Phase Error Tracking Control (ZPETC) is added to the system to track the reference input more precisely. The overall mechanism is manufactured using Electro Discharge Machining (EDM) to be used in experiments. The control system is empirically realized and results such as sinusoidal and step responses are evaluated in time domain for each controller separately. All the findings including amplification ratio and controller performance of each control algorithm are validated and evaluated using experimental setup with proper instrumentation.

Keywords: Precise position control, Compliant mechanism, Piezoelectricity, Bouc-Wen model, ZPETC

ÖZ

ESNEK MEKANIZMA VE PIEZO EYLEYİCİ VASITASI İLE TEK EKSENLİ HASSAS POZİSYON KONTROLÜ

YAŞAR, Gökhan
Yüksek Lisans, Makina Mühendisliği Bölümü
Tez Yöneticisi : Prof. Dr. Tuna Balkan
Ortak Tez Yöneticisi : Prof. Dr. Yavuz Yaman

Eylül 2013 , 72 sayfa

Bu çalışmada, piezo eyleyici vasıtasıyla tek eksenli hassas konumlama yapılmıştır. Piezo eyleyicinin düşük deplasman çıktısı sebebiyle, bu çıktıyı artıracak mekanik yükseltici sisteme eklenmiştir. Mekanik yükseltici olarak elastik olarak bükülebilen mafsallardan oluşan esnek bir mekanizma tasarlanmıştır. Tasarım farklı alternatiflerin belirli bir puanlamaya altında değerlendirilmesi sonucu kararlaştırılmıştır.

Mekanik yükselticinin tasarım parametreleri optimum olarak belirlenmiş ve oluşturulan sistemin statik analizleri sonlu elemanlar yöntemi kullanılarak gerçekleştirilmiş ve doğrulanmıştır. Sistemde histeri etkisini elemine etmek amacıyla Bouc-Wen modeli kullanılarak ileri beslemeli bir kontrol sistemi tasarlanmıştır. Buna ek olarak, referans girdi ve elde edilen çıktı arasındaki konum hataları, sisteme oransal ve tümlevsel (PI) tip geribesleme denetim kontrol sistemi eklenerek azaltılmıştır. Ayrıca, Sıfır Faz Hata Takip Kontrolü (SFHTK) sisteme eklenmiş ve sistemin referans girdiyi daha hassas takip etmesi amaçlanmıştır.

Tasarlanan mekanizma, tel erezyon yöntemi ile üretilmiştir. Üretimi takiben, oluşturulan deney düzeneği ile analitik ve sonlu elemanlar yöntemi ile bulunan yükseltme oranı doğrulanmıştır. Buna ek olarak tasarlanan kontrol algoritmaları sinus ve basamak girdileri kullanılarak denenmiş ve nihai sistem kararlaştırılmıştır.

Anahtar Kelimeler: Hassas konum kontrolü, Esnek mekanizmalar, Piezoelektrik malzemeler, Bouc-Wen modeli, ZPETC

to my Family

ACKNOWLEDGMENTS

I would like to express my sincere gratitude to my advisor, Prof. Dr. Tuna Balkan, for his guidance, support and technical suggestions throughout the study. I would like to express my gratitude to my co-advisor Prof. Dr. Yavuz Yaman for his support throughout the development of the conducted studies. I would also like to express my sincere appreciation for Furkan Luleci, Ozan Gerger, Cemal Saralp and Deniz Mutlu for their valuable friendship, motivation and help. For their understanding my spending lots of time on this work, my sincere thanks go to my family.

TABLE OF CONTENTS

LIST OF TABLES

TABLES

LIST OF FIGURES

FIGURES

NOMENCLATURE

A	Maximum Extension of A Piezoactuator
α	Rotation of Flexure About z Axis
b	Width of a Flexure
b_{damp}	Damping of The Mechanism
c	Compliance
D	Electrical Displacement
Δx	Displacement of Flexure About x Axis
Δy	Displacement of Flexure About y Axis
E	Electric Field
ϵ	Dielectric Permitivity
F_x	Force on Flexure in x Axis
F_y	Force on Flexure in y Axis
G_{cl}	Closed Loop Transfer Function
$G_{openloop}$	Open Loop Transfer Function
G_{zpetc}	Inverse Feedforward Model (ZPETC)
h	Hysteresis Factor of Piezoactuator
K	Stiffness
K_{in}	Input Stiffness of Overall Mechanism
K_{pzt}	Input Stiffness of Piezoactuator
l_a	Length of the Arm of The Mechanism
R	Radius of A Circular Flexure Hinge
R_{amp}	Amplification Ratio of The Mechanism
S	Mechanical Strain in Piezo
σ_r	Bending Stress on A Flexure Hinge
σ_t	Tensional Stress on A Flexure Hinge
T	Mechanical Stress in Piezo
t	Minimum thickness of A Circular Flexure Hinge
u	Input (V) to The Piezoactoator
VAF	Percent Variance for Account Criteria
y	Output Signal

CHAPTER 1

INTRODUCTION

1.1 Description of The Problem and Motivation of The Study

In the last few years, a growing interest has been devoted to precise positoning. Microelectromechanical systems (MEMS), scanning electron microscope (SEM), optical alignment and ultra precision machining could be given as examples where precise positioning is crucial. In addition to the technologies demanding precise positioning, tools for designing and manufacturing of the precise positioners are developing in a similar fashion as well. These tools include actuators with almost nanometer resolution and mechanisms with minimum possible backlash, sticktion, friction, etc. In this study, piezoactuators are chosen as the precise actuator and compliant mechanism is selected and investigated in detail.

Piezoactuators are one of the substantial candidate to be used in precise positioning. They can well meet the growing requirements of precise positioning such as nanometer resolution on motion, fast response and high stiffness values. Despite the important advantages for piezoactuators explained before, there are some downsides for piezoactuators as well. The limited displacement output and hysteresis between the displacement and applied electric field could be given as two main significant disadvantage. Various control algorithms are offered in literature to solve the hysteresis problem. In addition, some mechanical amplification mechanism are being used to solve the limited displacement output. As can be seen in Figure 1.1, Physik Instrumente® P-733 could be given as an example for a commercial product with single axis nanometer resolution precise positioner which uses a mechanical displacement amplifier and sophisticated control system on it.

In this thesis, it is intended to design a precise positioning mechanism to be used for a wide range of applications including position tracking in a specific displacement range and alignment of a body to another body for a specific position input. The designed mechanism is actuated with a piezoactuator and the input of piezoactuator is amplified with a mechanism which is composed of flexure hinges.

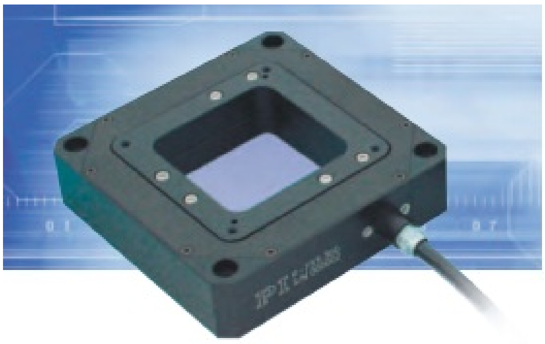

Figure 1.1: A Commercial Product for Precise Positioning [1]

1.2 Scope of The Thesis

In this study, the main subject is to design a precise positioning system which can be used for tracking and alignment purposes. In this manner, the range of the mechanism is to be high enough to be able to track wide range of inputs. Ihe range is decided to be 200 microns initially. Furthermore, the resolution of the overall system is to be as low as possible in order to reach the ultimate precision. Moreover, the control system on the work should be accurate enough to track the input precisely and to reach an error as low as possible. In the light of the above scope the basic concepts which are used during design process such as, piezoactuators, compliant mechanisms and the corresponding literature survey are presented in the remaining part of the current chapter. The detailed mechanical design is presented in Chapter 2. This chapter includes the comparison matrix analysis of different mechanisms which can be offered to solve the given problem and evaluation of them, the mechanical optimization procedure of the chosen mechanism, the finalized mechanical design which includes the consideration of manufacturing process and mounting of mechanism. Chapter 3 includes the control system design and experimental analysis. The mechanical design parameters such as amplification ratio and mathemetical models obtained analytically and by using FEM are compared with the experimental findings in this chapter. In experiments, the system identification is performed and the mathematical model of the overall system is obtained. Alternative control systems are offered to reach the maximum precision and these algorithms are implemented on a prototype system. Finally, an overall summary of the work done is presented in Chapter 4.

1.3 Background and Literature Review

1.3.1 Introduction

As explained in the previous sections, a precise positioning system is aimed to be designed. A precise positioning system comprises of a mechanism to manipulate the motion and an actuator is to deliver the motion. The purpose is to reach the most efficient tracking capability and steady state error for alignment purposes.

Unique fine resolution actuators and mechanisms should be designed to procure key requirements of the precise positioning duty. The traditional mechanisms which consist of rigid links and kinematic pairs are the most common way for position control. However, these kind of mechanisms have some disadvantages. The ball screws and roller bearings in traditional mechanisms suffer from backlash and stick-slip friction, in addition to that the assembly complication is another drawback for these elements. However, an interesting approach to solve this issue is proposed by Kim and Trumper [2]. Magnetic levitation (mag-lev) is developed to improve the precision by eliminating the dynamic effect such as backlash and friction on a traditional mechanism. However, this solution has its own drawbacks such as thermal dissipation problems, high cost etc.

Actuators are the other main part of a positioning system. Standard linear motors have a definite resolution and the cost rises as the precision desired is increased. Piezoactuators are used to solve this drawback as the piezoactuators have infinite resolutions in theory. However, they have very low displacement output. In order to solve this problem, a compliant mechanism is designed and the piezoactuator is integreted on this mechanism. The main duty of the mechanism is to amplify the motion with the minimum accuracy loss.

1.3.2 Compliant Mechanisms

Mechanisms can be defined such that mechanical devices that are used to deliver force, motion or energy in a mechanical system. According to this definition, the traditional mechanisms consists of rigid links and joints to transfer the above mentioned elements. Most common joints to transfer motion is the rotational joint. However, the most common problem encountered when these joints are used is, stick-slip friction, sometimes known as dry friction, and backlash etc. This problem gains importance especially in ultra precision positioning system with especially micrometer or nanometer resolutions since the motion is discontinuous at zero velocity [3].

In addition to above problems it would be very hard to assemble the micro mechanisms built by the traditional mechanisms (the joint assemble, actuator assemble etc). Asymmetric structure of mechanisms makes it sensitive to thermal strain errors. These errors require high cost to compensate. Therefore, for high precision systems another type of joint is developed and called flexure hinges. The mechanism which consists of flexure hinges is called compliant mechanism. In these mechanisms flexures creates the motion between two rigid links through elastic deformation of material itself as can be seen in Figure 1.2 and Figure 1.3 The compliant mechanism first used in history as bows and catapults. The kinetic energy is stored in bow or catapult is transferred to the arrow and heavy stone to propel them to long distances. In addition, the compliant mechanisms are very common in daily life today. Safety belt connectors, paper clips, nail scissors etc. are the examples of daily usage of compliant mechanism and some other examples can be found in Figure 1.4. In Figure 1.5 there are some other examples of compliant mechanisms which includes crimping mechanisms, motion amplification mechanisms and some limited rotation mechanisms. Burns and Crossley [6] studied

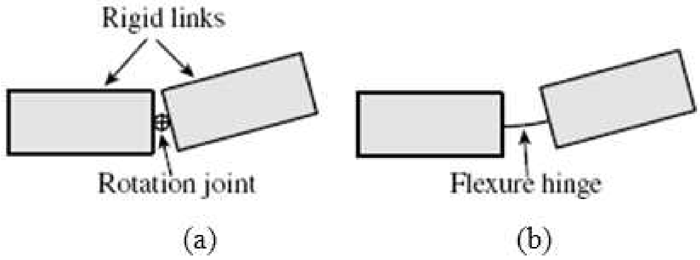

Figure 1.2: Joints Used in Mechanisms (a) Bearing Joint; (b) Flexure Hinge [4]

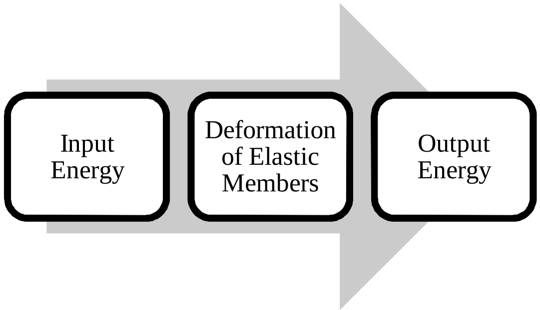

Figure 1.3: General Procedure of Compliant Mechanisms [4]

the very early in the area of compliant mechanisms. The encountered some difficulties about closed form solutions using kinetostatic analysis and synthesize the compliant mechanisms. Soup and McLaran [7] used the elliptical integral equations to obtain initial approximation for analyzing the compliant mechanisms. Midha and Howell [8] has published works about mobility of compliant mechanisms. The “compliance” term was first arrised in these works. Solomon [9] published a work investigating the general design process for compliant mechanism design. This method is similar to traditional mechanism investigation. The overall mechanism is chosen as rigid links and the compliance term is selectively added to the flexure points. Nahvi [10] worked on the dynamics of compliant mechanisms and proposed the use of eigenvalues of the stiffness matrix. In this way the mobility of compliant mechanism is indicated. Midha and Howell [8] developed the “pseudo rigid body model” as a kinematic model accepting cantilevered flexible elements with end force loading which is a combination of a force and a moment. After this work the pseudo rigid body model is used to obtain a loop closure equation and the investigation of the compliant mechanism became more efficient.

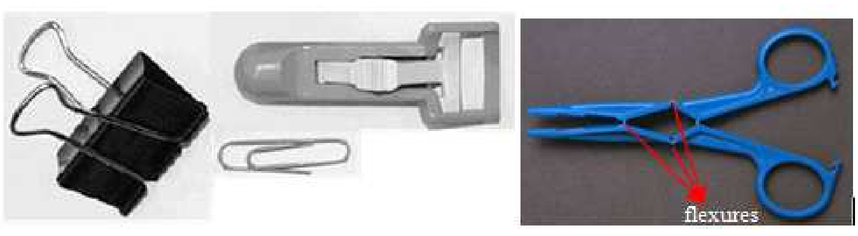

Figure 1.4: Examples of Compliant Mechanisms [5]

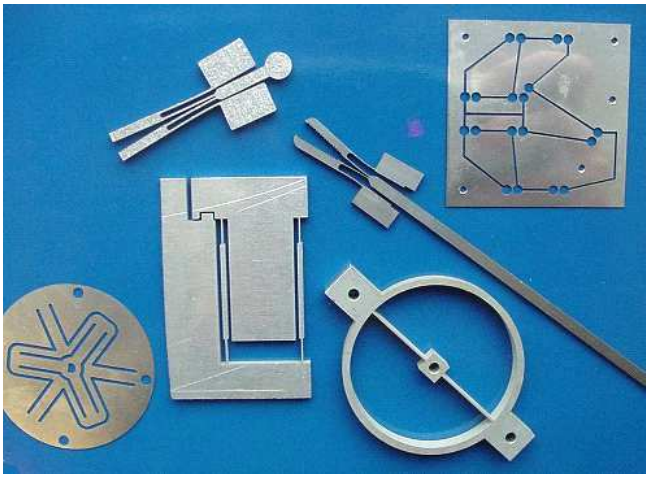

Figure 1.5: Some Compliant Mechanisms [5]

After pseudo-rigid-body model has been improved. Some empirical and analytical formulas have been put forward which is investigated in detail in Chapter 2.

1.3.3 Types of Flexures and Compliant Mechanisms

Lobontiu [4] divided the flexure types into three as in Figure 1.6 which includes single axis, two axis and multiple axis. Single axis flexure hinges in Figure 1.7(a) are designed to be

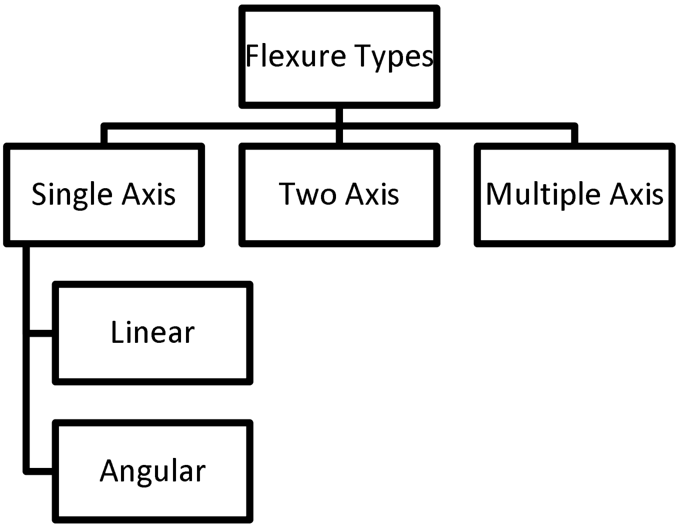

Figure 1.6: Types of Flexures

compliant in one direction that is, the elastic deformation of the geometry is sensitive to one direction only. These kind of flexures are used in planar applications. Two axis flexures as in Figure 1.7(c) enable bending and the corresponding relative rotation about two perpendicular axis at different spring constants. Multiple axis flexures as in Figure 1.7(b) have a rotation center at the thinnest section of the structure. However this thinnest section does not have any specific orientation as in the case of single axis and therefore they can be used in three dimensional applications where the direction of rotation is not important.

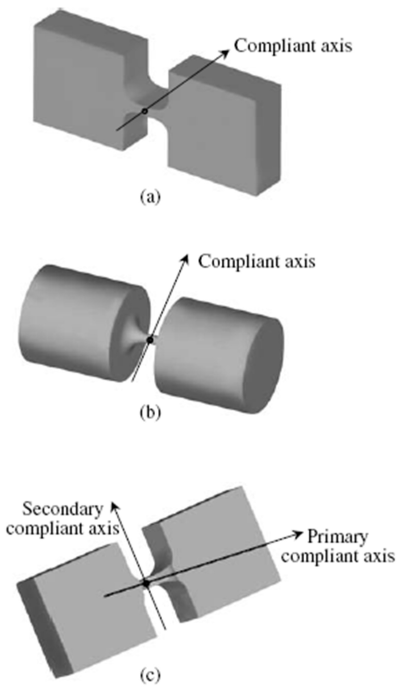

Figure 1.7: (a) Single Axis, (b) Multiple axis, (c) Two axis Flexures [4]

1.3.4 Advantages and Disadvantages of Flexures and Compliant Mechanisms

After all the detailed information given about flexure hinges and compliant mechanisms which is chosen as the mechanism to be used in the final system, the pros and cons of these mechanisms are also investigated against the traditional mechanisms consists of rigid links and joints. The advantages of compliant mechanisms can be listed as below;

- High precision can be obtained as the resolution of the flexures are infinite at theory (the resolution depends on the instrumentation of the overall system).

- There is no joints, bearings etc. Therefore no backlash and no need for lubrication.

- They are monolithic structures. There is no need for assembly as in traditional mechanism in Figure 1.8. Thus, there is less possibility of wearing the joints and less moving parts when compared to the traditional mechanism. Therefore, maintenance requirement is less.

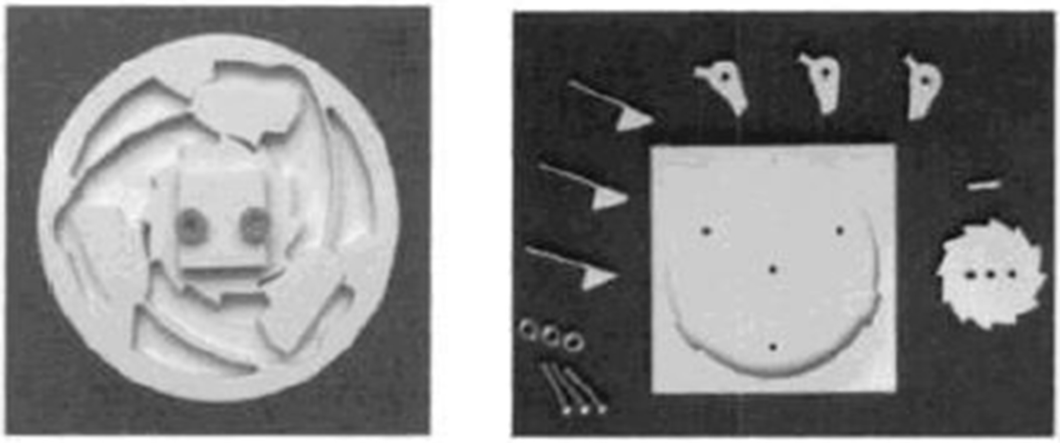

Figure 1.8: (a) Monolithic Compliant Mechanism, (b) The Assembled Traditional Mechanism [5]

- If the symmetry is used in compliant mechanism, the overall system becomes insensitive to disturbances such as temperature expansion etc [3].
- They can be controlled easily since the motion of the mechanism can be obtained from the known forces at the flexures using well defined pseudo-rigid-body model [11].
- Since the compliant mechanisms are monolithic, they can be scaled down very easily. In this way, micro-mechanisms can be produced and used in MEMS applications.

In addition to the above explained advantages, there are , naturally, disadvantages of compliant mechanisms and they are listed below;

- The most important disadvantage of the compliant mechanism is that it is hard to analyze these kind of mechanisms when compared to the traditional mechanisms. Even the latest developed technique pseudo-rigid-body model is used there are still some approximations and ignorance and as a result some faults are encountered. In addition, more mathematical work is required for a force analysis on these mechanisms.
- The movement of the compliant mechanism depends on the elastic deformation of the material. Therefore, the material selection is important and the solution depends on the material itself. In addition, if the chosen material exceeds the elastic range, the mechanism can not come back to the initial position. Moreover, in case a brittle material is chosen as the mechanism, there is a possibility of a sudden failure under heavy duty.
- The actuator mounting is to be performed carefully otherwise buckling and/or outplane motions could be encountered. The drive axis should be collinear with the direction of motion since the outplane stiffness is low whereas the drive direction stiffness is high.

1.3.5 Literature Review of Compliant Mechanisms

In literature, various compliant mechanisms are used to solve specific problem. Large deflection mechanisms, small deflection amplification mechanisms, heavy duty mechanisms etc. can be encountered in literature. Micro mechanisms are used in MEMS (Micro Electro Mechanical Systems) applications. The size of these mechanisms are in micron scale and they are manufactured using special techniques. Garcia [12] published a work in Sibley School of Mechanical and Aerospace Engineering about a mechanism that is capable of transforming the input from a thermal actuator into an amplified displacement. This mechanism which is shown in Figure 1.9 is designed to amplify the motion of thermal input. The mechanism

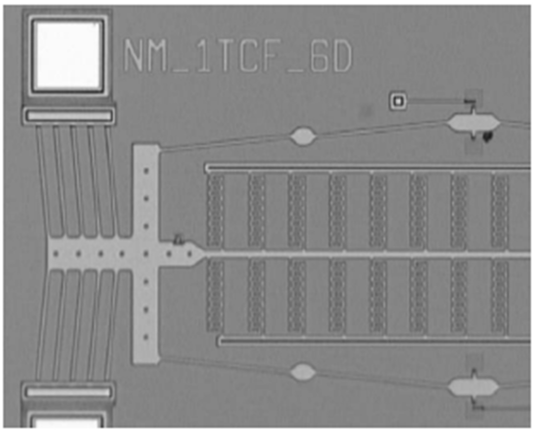

Figure 1.9: Thermally Actuated Micro Compliant Mechanism [12]

is comprised of flexure hinges and designed to increase the thermal expansion value in the same direction in micron scale. Zubir [13] designed a microgripper mechanism to complete the pick and place task. A hybrid flexure-based compliant mechanism as in Figure 1.10 is designed and a bias spring structure is included to design which consequently amplifies the input coming from pizeoactuator and grasping precisely property. In addition to compliant

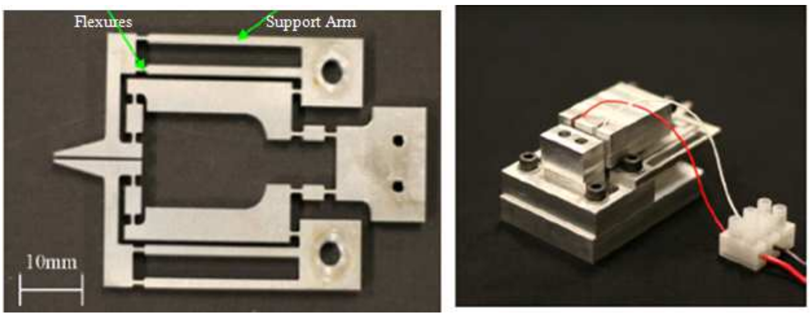

Figure 1.10: (a) Microgripper Mechansim, (b) Assambled Microgripper Mechanism [13]

mechanisms in small scale, there are some studies, in literature, dealing with large scale compliant mechanisms. Tanık [14] published a work on analysis and design of a compliant spatial four-bar mechanism which consists of a traditional spherical joint and a flexure hinge. The mechanism which can be seen in Figure 1.11 is capable of possessing out of plane motions.

The analysis and design guide of such mechanisms is also investigated in the publication. All the design and analysis works are based on pseudo rigid body model approach.

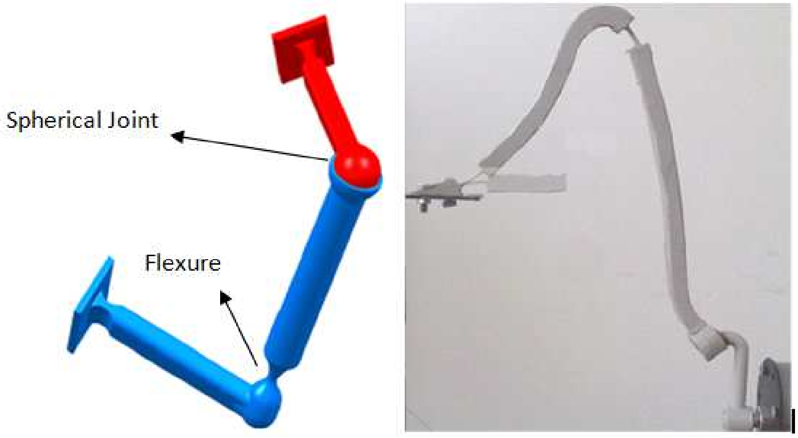

Figure 1.11: (a) Compliant Spatial Four-Bar Mechanism, (b) Manufactured Mechanism [14]

Subaşı [15] studied in Middle East Technical University on design of a compliant bistable four-link mechanism. The designed mechanism which can be seen in Figure 1.12 is implemented on door lock mechanism in commercial dishwashers. The designed mechanism is aimed to be replaced with a rigid inverted slider crank mechanism which operates with a spring force. The aim here is to get rid of the slider crank mechanism and the spring and reduce the cost of the overall dishwasher. In the final work, the spring is only reduced from the spring and the revolute joints are remained in the system. The removal of the revolute joints with the flexures is put as a future work. During the design, pseudo rigid body model is used. The cases where the precise positioning is main duty, more work is devoted in

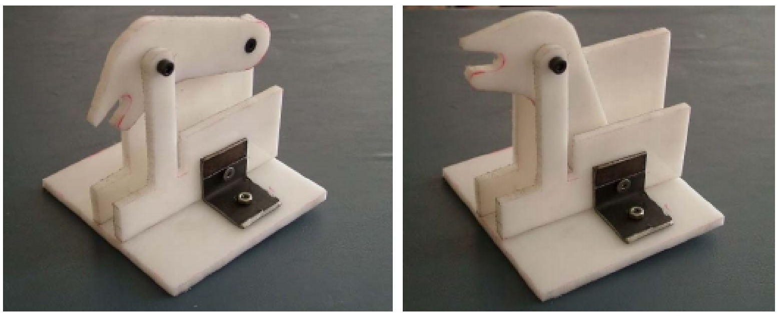

(a) (b)

Figure 1.12: Two stable positions of the prototype [15]

literature. Yang[16] designed a single axis precise position control mechanism consisting a piezoactuator and a compliant mechanism as in Figure 1.11. The mechanism is designed to be used in diamond turning. The work includes the general analytical equations for calculating the stiffness and displacement of the mechanism. The developed equations include the effects of rotation and stretching each of the flexure hinge. The difference between the improved analytical equations and finite element methods are very small and 3.1% for displacement and

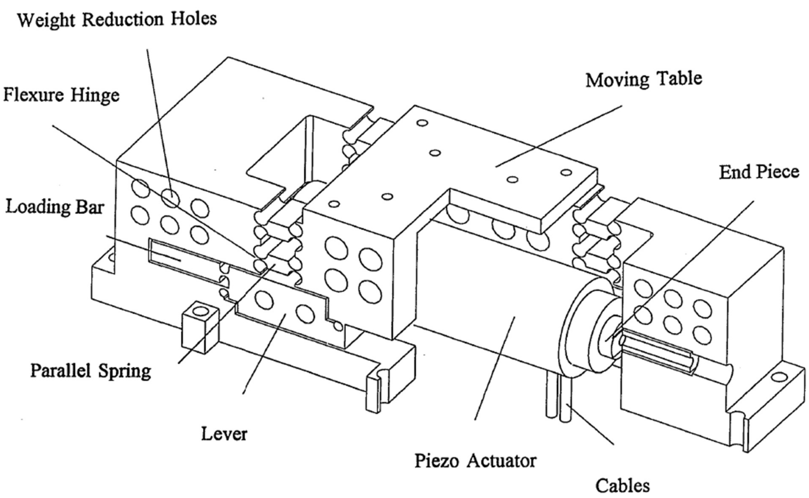

Figure 1.13: One Axis Micro-Positioning Stage [16]

1.3% for stiffness calculations. The overall mechanism is fabricated by using EDM (Electro Discharge Machining) and the produced mechanism differs from both analytical and finite element models in about 8%. Yao [17] designed a two axis precise positioning stage actuated by piezoactuators. The design includes a monolithic compliant mechanism with circular flexure hinges as in Figure 1.14. The piezoactuators in the system can work independently since the mechanism design is totally decoupled. The mechanism which has 87m x 87m working zone and 20nm resolution is designed to be kinematically determinate. The overall mechanism is produced using EDM and stainless steel. Tjiptoprodjo [18] designed a piezoactuator

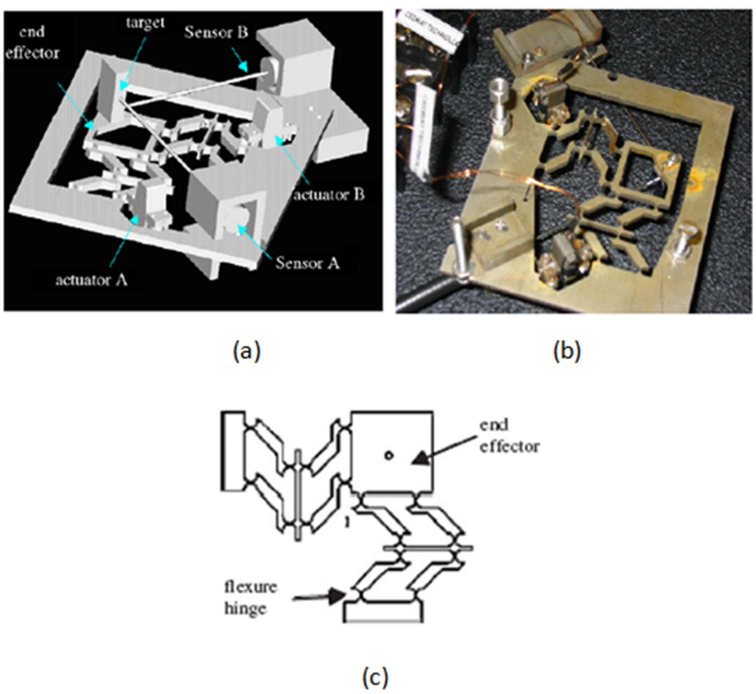

Figure 1.14: The Micro-Positioner (a) Solid Model, (b) Real Stage, (c) Schematic Diagram of Mechanism [17]

driven $xy\theta$ platform. The movement of the mechanism which is given in Figure 1.15 is in x and y directions and in addition to that the mechanism is able to rotate about the plane of motion. Finite element model of the overall system including piezoactuators are improved in ANSYS® by using specific elements having the property of coupling (the mechanical and electrical properties of the elements are coupled. By this way a more accurate finite element model is obtained capturing the all physical behavior of the piezoactuators. The piezoactua-

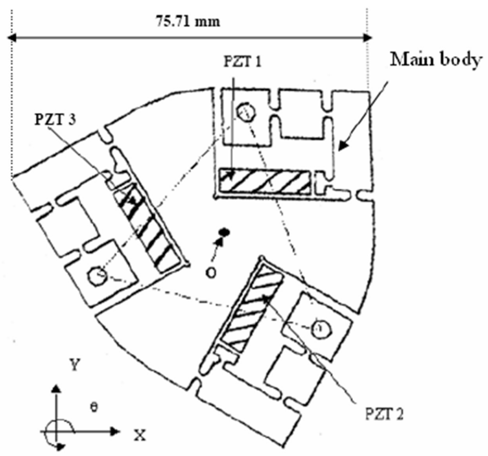

Figure 1.15: Schematic Diagram of the Mechanism [18]

tors mounted to the system is prestressed and in this way the accuracy of the overall system is increased. However, the asymmetry of the mechanism can lead to considerable uncertainty.

1.4 Piezoactuators

1.4.1 Piezoelectricity

Piezoelectric materials which has ability to couple the electrical and mechanical properties and gives response to both electric charge as mechanical stress and mechanical stress as electric charge have a common use in today's technology. This kind of materials are first discovered by Jacques and Pierre Curie in 1880s. The first foundation of these material was the electric charge obtaining when the applied load is applied to the material. This relation is called as "direct piezoelectric effect". The inverse of this phenomena which is the mechanical stress obtaining when electric charge is give to the system is "converse piezoelectric effect". This property gives the piezomaterials the ability to be used both as sensors and actuators as in Figure 1.16 [19]. In nature there are various materials having the property of piezoelectricity. Lead zirconate titanate (PZT) is the most common piezo material as synthetic materails. In addition to that polymer based polyvinylidene fluoride (PVDF), barium titanate can be given as the other synthetic piezoelectric materials. Ammonium phosphate and quartz can be given as examples of natural piezomaterials. In this work the piezomaterials is used as actuators. In this manner, the material should have high stiffness and high travel range. Piezoactuators

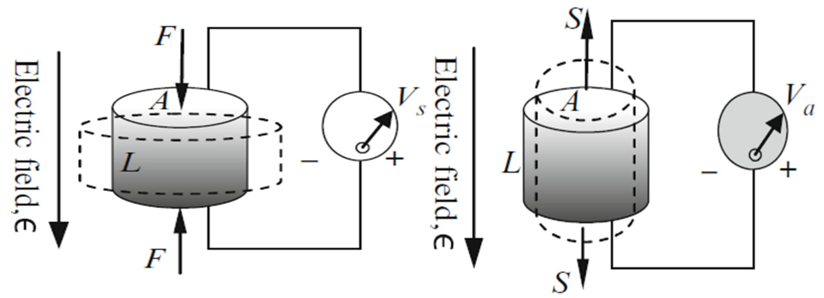

Figure 1.16: (a) Direct Piezoelectric Effect, (b) Converse Piezoelectric Effect [19]

have very low actuation capabilities except piezostacks. Piezoactuatros in stack configiration have piezo layers on top of each other and in this way the actuation capacity is increased upto 0.1% of the length of the piezostack [19]. Therefore, PZT materials are chosen with stack configration as the actuator in this work. The detailed investigation about piezo stack actuators are given in the following sub-chapter in detail.

1.4.2 Stacked Piezoactuators

Stacked piezoactuators are multilayer actuators in which many layer of PZT's are stacked on top of one each other as shown on Figure 1.17. If the volume of piezoelectric element

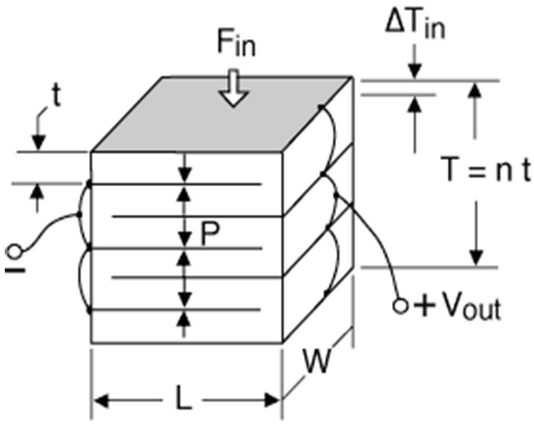

Figure 1.17: Stacked Piezoactuator [20]

increases, the energy that is delivered to a load is also increases. Therefore, the capacity of extension of the piezoactuator increases. However, as the number of layers increase the wiring of all the layers becomes a problem. As a result, the construction of the stack actuators are limited. Polarization is the key point in piezoelectric materials which gives the coupling properties as mentioned previously. Figure 1.18 denotes the different direction and orientation axis of a typical piezoelectric material. Axis 1, 2 and 3 denote the typical right hand ruled three axis (X,Y,Z). 4,5 and 6 denote the rotation about the three axis. The direction of polarization is along axis 3 and in stacked actuators the layers are constructed along axis 3 and two electrodes are mounted on the very top and very bottom layer. As a result of an

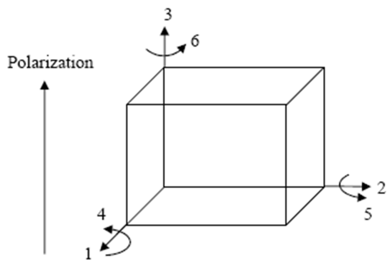

Figure 1.18: Direction and Orientation Axis of Piezo Materials

electric field application to these electrodes the deformation occurs in the direction of axis 3. This direction and orientation definitions will be used in further formulations of piezoactuator motion for further analysis in this study.

1.4.3 Definitions of Piezostack Properties

The mechanical and electrical coupled property of a piezoelectric material is based on Eq(1.1) and Eq(1.2);

$$S = c^E T + dE \tag{1.1}$$

$$D = dT + \varepsilon^T E \tag{1.2}$$

where c denotes the inverse of stiffness (compliance), S and T denotes the mechanical strain and stress D, E and ϵ denotes the electrical displacement, electrical field and dielectric permittivity of the material, respectively. From the above equations the coupling property of piezoelectric materials can be seen. From Figure Figure 1.18, The piezoelectric relations Eq(1.1) and Eq(1.2) can be written in three dimensional form as follows [18];

$$\begin{bmatrix} S_1 \\ S_2 \\ S_3 \\ S_4 \\ S_5 \\ S_6 \end{bmatrix} = \begin{bmatrix} s_{11}^E & s_{12}^E & s_{13}^E & s_{14}^E & s_{15}^E & s_{16}^E \\ s_{21}^E & s_{22}^E & s_{23}^E & s_{24}^E & s_{25}^E & s_{26}^E \\ s_{31}^E & s_{32}^E & s_{33}^E & s_{34}^E & s_{35}^E & s_{36}^E \\ s_{41}^E & s_{42}^E & s_{43}^E & s_{44}^E & s_{45}^E & s_{46}^E \\ s_{51}^E & s_{52}^E & s_{53}^E & s_{54}^E & s_{55}^E & s_{56}^E \\ s_{61}^E & s_{62}^E & s_{63}^E & s_{64}^E & s_{65}^E & s_{66}^E \end{bmatrix} \begin{bmatrix} T_1 \\ T_2 \\ T_3 \\ T_4 \\ T_5 \\ T_6 \end{bmatrix} + \begin{bmatrix} d_{11} & d_{21} & d_{31} \\ d_{12} & d_{22} & d_{32} \\ d_{13} & d_{23} & d_{33} \\ d_{14} & d_{24} & d_{34} \\ d_{15} & d_{25} & d_{35} \\ d_{16} & d_{26} & d_{36} \end{bmatrix} \begin{bmatrix} E_1 \\ E_2 \\ E_3 \end{bmatrix} \tag{1.3}$$

$$\begin{bmatrix} D_1 \\ D_2 \\ D_3 \end{bmatrix} = \begin{bmatrix} d_{11} & d_{12} & d_{13} & d_{14} & d_{15} & d_{16} \\ d_{21} & d_{22} & d_{23} & d_{24} & d_{25} & d_{26} \\ d_{31} & d_{32} & d_{33} & d_{34} & d_{35} & d_{36} \end{bmatrix} \begin{bmatrix} T_1 \\ T_2 \\ T_3 \\ T_4 \\ T_5 \\ T_6 \end{bmatrix} + \begin{bmatrix} \varepsilon_{11}^T & \varepsilon_{12}^T & \varepsilon_{13}^T \\ \varepsilon_{21}^T & \varepsilon_{22}^T & \varepsilon_{23}^T \\ \varepsilon_{31}^T & \varepsilon_{32}^T & \varepsilon_{33}^T \end{bmatrix} \begin{bmatrix} E_1 \\ E_2 \\ E_3 \end{bmatrix} \tag{1.4}$$

The above equations can be rewritten again by considering the linear isotropy phenomena in ANSI/IEEE Standard 176-1987 [21] as follows;

$$\begin{bmatrix} S_1 \\ S_2 \\ S_3 \\ S_4 \\ S_5 \\ S_6 \end{bmatrix} = \begin{bmatrix} s_{11}^E & s_{12}^E & s_{13}^E & 0 & 0 & 0 \\ s_{21}^E & s_{22}^E & s_{23}^E & 0 & 0 & 0 \\ s_{31}^E & s_{32}^E & s_{33}^E & 0 & 0 & 0 \\ 0 & 0 & 0 & 0 & 0 & 0 \\ 0 & 0 & 0 & 0 & s_{55}^E & 0 \\ 0 & 0 & 0 & 0 & 0 & 2\left(s_{11}^E - s_{12}^E\right) \end{bmatrix} \begin{bmatrix} T_1 \\ T_2 \\ T_3 \\ T_4 \\ T_5 \\ T_6 \end{bmatrix} + \begin{bmatrix} 0 & 0 & d_{31} \\ 0 & 0 & d_{31} \\ 0 & 0 & d_{33} \\ 0 & d_{15} & 0 \\ d_{15} & 0 & 0 \\ 0 & 0 & 0 \end{bmatrix} \begin{bmatrix} E_1 \\ E_2 \\ E_3 \end{bmatrix} \tag{1.5}$$

$$\begin{bmatrix} D_1 \\ D_2 \\ D_3 \end{bmatrix} = \begin{bmatrix} 0 & 0 & 0 & 0 & d_{15} & 0 \\ 0 & 0 & 0 & d_{15} & 0 & 0 \\ d_{31} & d_{32} & d_{33} & 0 & 0 & 0 \end{bmatrix} \begin{bmatrix} T_1 \\ T_2 \\ T_3 \\ T_4 \\ T_5 \\ T_6 \end{bmatrix} + \begin{bmatrix} \varepsilon_{11}^T & 0 & 0 \\ 0 & \varepsilon_{22}^T & 0 \\ 0 & 0 & \varepsilon_{33}^T \end{bmatrix} \begin{bmatrix} E_1 \\ E_2 \\ E_3 \end{bmatrix} \tag{1.6}$$

With the Eq(1.5) and Eq(1.6) and the given properties supplied by the manufacturer a piezoelectric element can be modeled analytically to investigate further.

1.4.4 Advantages and Disadvanteges of Piezoactuators

The selection of piezoactuators in the defined problem depends on some evaluation and these evaluations are based on the advantages and disadvantages of piezoactuators in use, the advantages of the piezoactuators can be written as follows;

- Piezoactuators does not produce magnetic field during operation as the traditional actuators. They only produce electrical field and this property makes the piezoactuator very suitable for precise positioning of electrical devices. The system, for example, can be designed to be used during antenna measurements. In this way, the precise positioning operation can be complated without effecting the antenna performance.

- Piezoelectric actuators can produce extremely fine position changes down to sub nanometer range. The resolution of the actuators depends on the other instruments used in the system such as the power amplifier, the sensor etc. [18].

- Piezoactuators uses the electric field to produce motions. The load carried is not related to the acutator's power. Therefore, carrying high loads does not consume power [22].

- Piezoactuators does not need any lubricants for maintenance and there are no wear and abrasion during motion [19].

There are some disadvantages of these kind of actuators as well. However, these limitations could be ignored considering the purpose and the strength of them. The disadvantages can be written as follows;

- Piezoactuators are much harder to control when compared to traditional actuators. They produce nonlinear hysteretic behavior and conventional control algorithms may not enough to control the system depending on application.

- Piezoactuators gives very small displacement values (approximately 0.1% of the length of the actuator itself [19]. Therefore in case where more displacement is required an amplifying mechanism is to be considered.

CHAPTER 2

DESIGN OF ONE AXIS COMPLIANT MECHANISM

In this chapter, it is intended to give information about key points used during design process of compliant mechanism which is desired to amplify the limited input coming from the piezoactuator. An initial alternative evaluation is performed. Following that, according to chosen type of mechanism, some basic design rules which is pseudo rigid body model, stress consideration, amplification ratio derivation, optimization of amplification ratio using and PZT mounting design steps are followed.

2.1 Design Alternative Evaluation

For precise positioning some alternative mechanisms are used both to amplify the small displacement output of the piezoactoator and precise positioning in literature. In order to decide the bet alternative, a weight chart is constructed and each of the alternatives which are Scott-Russel mechanism, topologically optimized mechanism and Bridge type mechanism is evaluated respectively. The Scott–Russell mechanism is the simple structure with the main feature of displacement amplification and straight-line motion with right angle direction change of the input motion as in Figure 2.1 [23]. The mechanism itself can be modeled as a slider and

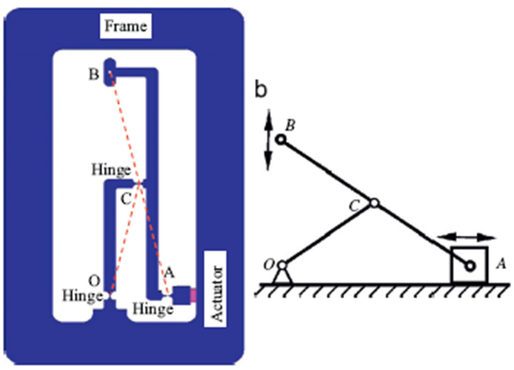

Figure 2.1: Schematic Diagram of Scott-Russel Mechanism [23]

crank mechanism with the slider being the precise positioned interface. Major drawback of this mechanism is that the precision can be low when the slider is not guided as in the case of slider crank mechanism. However, the guiding could also be regarded as a limitation since the friction becomes a problem to deal with.

Moonie type of mechanisms [24] are flextensional transducers which consist separate specifically designed metal end caps and a piezoactuator bonded to this metals as given in Figure 2.2. The most important advantage of these mechanisms is that the structure uses the axial extension of the piezoactuator in addition to the linear extension. In this way the amplification ratio is magnified. On the other hand, the bonding of the metals to the piezoactuator is a hard to implement and the property of the used adhesive depends the use environment, cycle time etc. which limits the use of the system. In addition, the amplification ratio depends

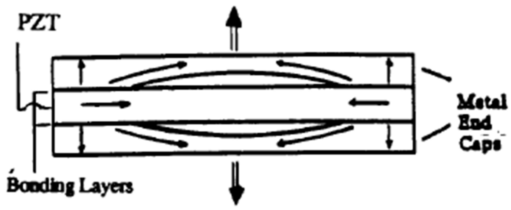

Figure 2.2: Schematic View of Moonie Type Actuator [24]

on the diameter of the cavity of the mechanism which is very hard to model and investigate analytically.

Bridge type mechanisms have simple structures and yet, a symmetric design with a lever in each quarter of it as in Figure 2.3. The motion of the actuator is amplified by using the lever

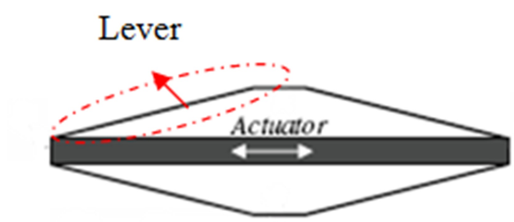

Figure 2.3: Schematic Diagram of Bridge Type Mechanism

and is converted to the perpendicular axis. The bridge type mechanisms are symmetric in two axis and in this way the accuracy of the overall mechanism is not affected from disturbances such as thermal expansion and misalignment of actuator. The integration of these mechanisms to real systems are more practical when compared to the previous two candidates since bonding of the piezoactuator is not required. The amplification ratio, on the other hand, is lower than the other two since the perpendicular axis of piezoactuator is not being used.

Bimorph Based Double Amplifier mechanism uses both bending and flextensional features of the material to produce the displacement [22]. Contrary to the previous three types, this mechanism consist of two actuators. As given in Figure 2.4 the actuators in this mechanism can be a piezoactuator actuator or another commercial linear actuator. This mechanism is pretty good with the motion amplification with two actuators mounted, however, synchronizing two actuators without coupling is a hard issue when the control system is concerned. Moreover, mounting of two actuators is another problem when the mechanical design is of concern. Another motion amplification mechanism among the alternatives is the Pyramid

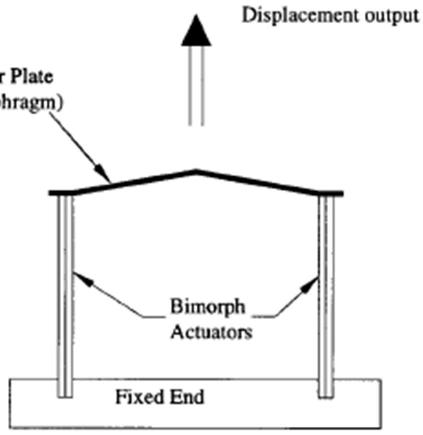

Figure 2.4: Schematic View of Bimorph-Based Double-Amplifier Mechanism [22]

Actuator Mechanism. Similar to Bimorph Based Double Amplifier mechanisms, Pyramid Actuator mechanisms also include two actoators. As in Figure 2.5, the use of two actuators could increase the amplification ratio to a higher value. As in the case of bimorph-based

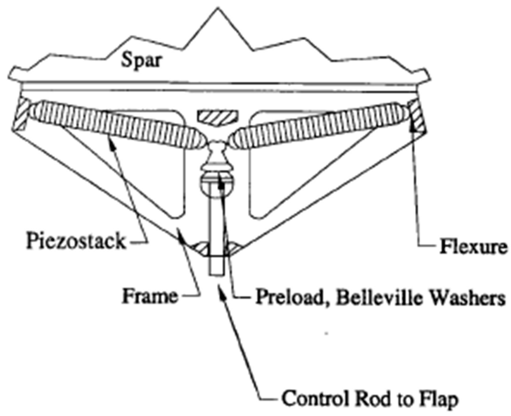

Figure 2.5: Schematic View of Pyramid Mechanism [22]

double-amplifier mechanism, the usage of two actuators for one dimension motion causes the synchronizing problem. Moreover mounting of two actuators is another problem when the mechanical design is of concern. All the decided five alternatives for the compliant mechanism design are evaluated (from 1:the worst to 5:the best) according to the following conditions;

- Range of Motion: The range of motion capability gives the overall system to align the subject in a wider dimensions.

- Precision: The precision for precise positioning is important. The overall system should have high repeatability and should not be affected to misalignments and disturbances such as thermal expansions.

- Ease of Fabrication: The manufacturing of the mechanism should be considered. Complex structures with very stick dimensional tolerances make the mechanism to be produced in more effort and cost.

Table 2.1: Evaluation Results of Three Alternatives

Type of Mechanism	**Scott Russel**	**Moonie**	**Bridge Type**	**Bimorph Based**	**Pyramid**
Range of Motion	4	5	4	5	5
Precision	4	3	5	3	3
Ease of Fabrication	5	5	5	5	4
Design Effort	5	3	5	1	1
Total	16	16	19	14	13

After the evaluation result given in Table 2.1, the bridge type is chosen to be the amplifying mechanism of the system and the design is performed according to this concept.

2.2 Proposed Mechanism Design

Piezoelectric actuator is chosen for the actuation of the linear positioning issue as they can produce high precision mechanical movement. The range of piezoactuators, on the other hand, are very limited. In order to widen the range of the overall system an amplification mechanism is to be designed. Therefore, the mechanism that is to be used in this system should have the property of amplifying the input displacement in addition not to have the resolution decreasing fetures such as friction, stiction etc.

- The mechanism should has a workspace as small as possible.

- The displacement range of the mechanism is to be at least 200 microns since the aim is to compensate the manufacturing tolerances.

- The minimum carrying capacity of the mechanism should be at least 200 grams.

- The motion is to be exactly on one axis so, the deviation of motion to another axis during the motion should not allowed.

- The stage should be robust, be stable at high frequencies (the power amplifier used in experiments decides the limit).

- The stage should be designed so that the manufacturing is as easy as possible.

By considering the above design requirements, the bridge type compliant mechanism as in Figure 2.6 is chosen to be designed as explained in the previous part in detail. The mechanism

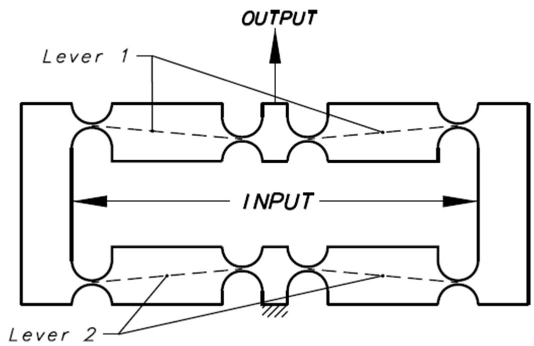

Figure 2.6: General View of Bridge Type Compliant Mechanism

in Figure 2.6 is symmetric in two axis which gives the advantage of pure one axis motion. In addition, there are two levers as of the offset between flexures at each quarters which amplifies the displacement coming from the piezoactuator. The amplification ratio of a typical bridge type mechanism is to be derived analytically by considering the elastic deformation of flexure hinges and using the pseudo-rigid body concept. This derived amplification ratio is to be compared with the experimental data. Besides, an additional design which may include the implementation of an interface to the mechanism. In this way the mechanism can be used for a special purpose. Moreover, mounting of the piezoactuator to the mechanism is needed.

2.3 Pseudo Rigid Body Model

Pseudo Rigid Body Model (PRBM) approach is an essential tool to model and analyze the compliant mechanisms. Howell and Midha [5],[8] developed and described the model first for application. In the model, the flexure hinge (the slenderized sections of compliant mechanism) is treated as a flexible link which is composed of torsional springs in the plane of motion as in Figure 2.7. As can be seen in Figure 2.8 the PRBM does define only the rotational motion about the axis perpendicular to the motion plane. According to Lobontiu [4], the shearing force and axial force have to be added to the model to model the structure correctly. In order to accomplish that, two other springs (each for the motion in one axis) are to be added to the system to define the motion as in Figure 2.8. A compliant mechanism can be modeled using the PRBM by simply assuming the parts of the mechanisms rigid, except the flexure parts. The flexure parts represent the stiffness of the overall system as springs. Each spring used defines the motion with a “stiffness” value which describes the transfer function of the spring displacement as the output and the force as the input. For the compliant mechanism applications, the input is the displacement and the output is the force and the I/O relationship is to be converted. This relation is called “compliance” and it is the inversion of the stiffness value as in Eq(2.1).

$$\begin{aligned} &F = ku \\ &\text{c=}\frac{1}{k} \;\Rightarrow\; u = cF \end{aligned} \tag{2.1}$$

where in the above equation k,c,u and F are stiffness, compliance, input and force respectively.

In order to model the compliant mechanisms using the PRBM, the compliance values have to be precise enough to compensate the stiffness of the overall mechanism. The stiffness is accepted to be lumped in the flexures. In addition, the flexure hinge geometry is important as the stiffnes is important and it affects the motion of the mechanism. For a rotaional motion, the circular flexure hinge is the best alternative since their center of rotation do not displace as much as other flexure hinges such as beam type [25] and corner filleted [26]. Therefore, the circular flexure hinges (notch flexure hinges) are chosen in this study. For the circular flexure hinges, there are many methods for finding the compliance value. Some researchers used

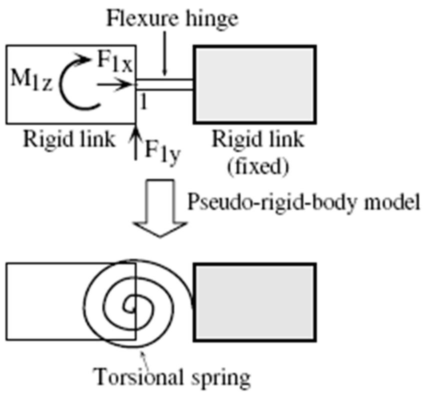

Figure 2.7: A Two Dimensional Flexure Hinge Model [5]

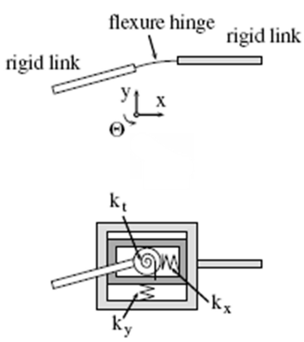

Figure 2.8: PRBM for A Planar Motion [5]

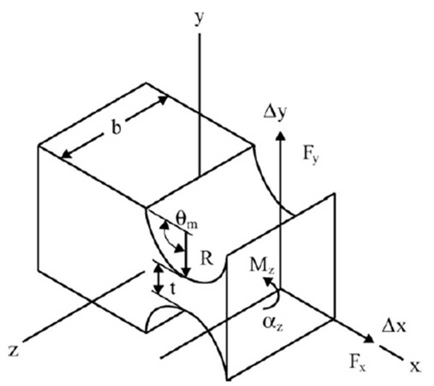

Figure 2.9: Circular Flexure Hinge General View [4]

the differential equation of a beam to derive the three compliance equations [27], some used Castigliano's second theorem [4] and some researchers derived empirical formulas to model the compliance values. Yong [25] combined all these studies and came up with a comparison of the methods with the FEA results by the t/R ratio in Figure 2.9.

For the rotational motion (rotational compliance) about $+z(\alpha_z/\mathrm{M}_z)$ in Figure 2.9 the percent errors changing by the t/R ratio can be found in Figure 2.10. Analyzing the Figure 2.10

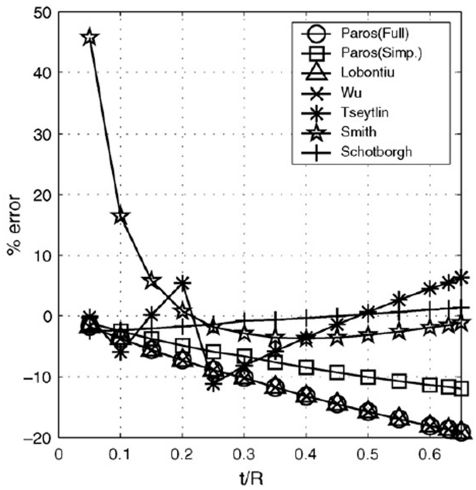

Figure 2.10: Percantage Errors of α_z/M_z Compared to FEA Results [11]

detailly, it can be said that Schotborgh [26] empirical method for α_z/M_z has the least error when compared to the FEM by considering the range $0.05 \leq$t/R≤ 0.65.

For the linear motion (the compliance values in x and y directions) the same study by Yong [25] is completed and the comparison of the models with FEA results can be seen in Figure 2.11.

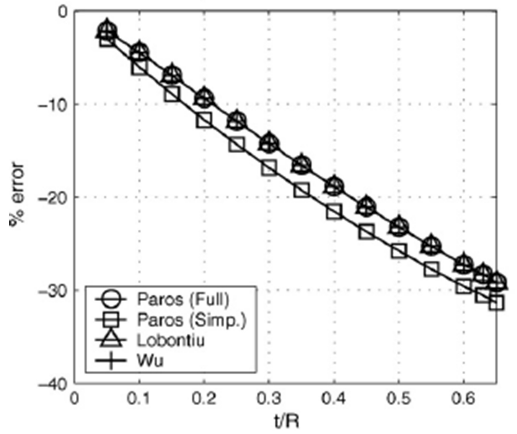

Figure 2.12: Percantage Errors of Δy/F$_x$Compared to FEA Results[11]

As can be seen from Figure 2.11 and Figure 2.12 Paros and Weisbord's full model [11] defines the compliance values with less error when compared with the FEA results. However there is a considerable error for these models and as the t/R ratio increases the error between FEA results rise up to 30%. The chosen compliance models for the three directions can be written as; Schotborgh model for α_z/M_z;

$$\frac{\alpha_z}{M_z} = \left\{ \frac{Ebt^2}{12} \left[-0.0089 + 1.3556\sqrt{\frac{t}{2R}} - 0.5227\left(\sqrt{\frac{t}{2R}}\right)^2 \right] \right\}^{-1} \tag{2.2}$$

Paros and Weisbord model for Δx/F$_x$ and Δy/F$_y$;

$$\frac{\Delta x}{F_x} = \frac{1}{Eb}\left[-2\tan^{-1}\frac{\gamma-\beta}{\sqrt{1-(1+\beta-\gamma)^2}} + \frac{2(1+\beta)}{\sqrt{2\beta+\beta^2}}\tan^{-1}\left(\sqrt{\frac{2+\beta}{\beta}}\frac{\gamma-\beta}{\sqrt{1-(1+\beta-\gamma)^2}}\right)\right\} \tag{2.3}$$

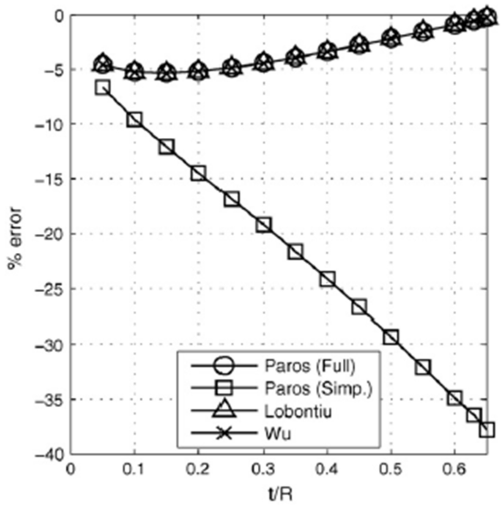

Figure 2.11: Percantage Errors of Δx/F$_x$Compared to FEA Results[11]

$$\frac{\Delta y}{F_y} = R^2 \sin^2\theta_m \left(\frac{\alpha_z}{M_z}\right) - \frac{3}{2Eb}\left\{\left[\frac{1+\beta}{(1+\beta-\cos(\theta_m)^2} - \frac{2+(1+\beta)^2/\left(2\beta+\beta^2\right)}{(1+\beta-\cos(\theta_m)}\right] \ldots \right.$$
$$\left. \sin\theta_m + \left[\frac{4(1+\beta)}{\sqrt{2\beta+\beta^2}} - \frac{2(1+\beta)}{(2\beta+\beta^2)^{3/2}}\right]\tan^{-1}\sqrt{\frac{2+\beta}{\beta}}\tan\frac{\theta_m}{2} - (2\theta_m)\right\} \tag{2.4}$$

where in the above equation, $\beta = \frac{t}{2R}$, $\gamma = 1 + \beta$, $\theta_m = \pi/2$. The mechanisms can be treated as a conventional mechanism with three springs attached to the joints as the 'Pseudo Rigid Body Model' is used and the compliance values of these joints (which are flexure hinges) can be found in above equations.

2.4 Stress Considerations of Flexure Hinges

During the design of flexure hinges, the stresses should be concerned since the thin sections in flexures define the motion and can cause a failure during motion. For a compliant mechanism the thinnest section is on flexure hinges (t×b) in crossection in Figure 2.13. Ling [28] defined

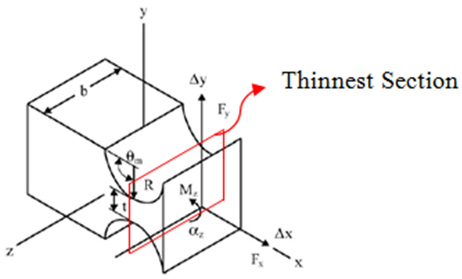

Figure 2.13: The Thinnest Section of A Flexure

the largest bending moment in a circular flexure hinge using Fourier integral methods and a solution for the stresses in a circular flexure hinge subjected to pure bending. Frocht [29] validated this finding experimentally using the photo-elastic studies and solution is given in terms of stress concentration factor K_t.

$$\sigma_r = K_t \frac{6M}{t^2 b} \tag{2.5}$$

where σ_r is the true stress and M is the applied bending moment. However, the stress concentration factor K_t and the applied bending moment M is unknown for many applications. Therefore, pseudo rigid body model could be used [30] while defining the bending moment for a flexure hinge as follows;

$$\sigma_r = \frac{E(1+\beta)^{9/20}}{\beta^2 f(\beta)}\theta_{\max} \tag{2.6}$$

where in above equation ;

$$\beta = \frac{t}{2R} \tag{2.7}$$

and,

$$\mathrm{f}(\beta) = \frac{1}{2\beta+\beta^2}\left[\frac{3+4\beta+2\beta^2}{(1+\beta)(2\beta+\beta^2)} + \frac{6(1+\beta)}{(2\beta+\beta^2)^{1.5}}\tan^{-1}\left(\frac{2+\beta}{2\beta+\beta^2}\right)^{0.5}\right] \tag{2.8}$$

Therefore, putting the maximum rotation value θ_{max} into Eq(2.6), the maximum bending stress in the flexure can easily be found. The linear stresses also occurs at compliant mechanism during motion. Looking at Figure 2.13 the thinnest section can be seen from the red slice shown there. The area of the thinnest section is (t×b) and the tensile stress occurs at this section is;

$$\sigma_l = \frac{AK_{in}}{bt} \tag{2.9}$$

Where A is the maximum stroke of the piezoactuator and K_{in} is the input stiffness of the mechanism which will be calculated later. The stress equations given above is to be used in designing a compliant mechanisms in order not to fail due to stress.

2.5 Analytical Derivation of Amplification Ratio

Let K_r and K_l be the rotational and directional stiffness values of each flexure hinge. Each flexure hinge in the mechanism has 2-DOF which are rotational and translational deformations. Other bodies except flexure hinges are accepted to be rigid. Once looking at the Figure 2.14, it can be seen that once a horizontal motion is given to the system, the vertical offset between flexures causes a rotation and the rigid parts of the mechanism translates. As a result, an output of Δy occurs. A detailed static force moment analysis is to be performed here to

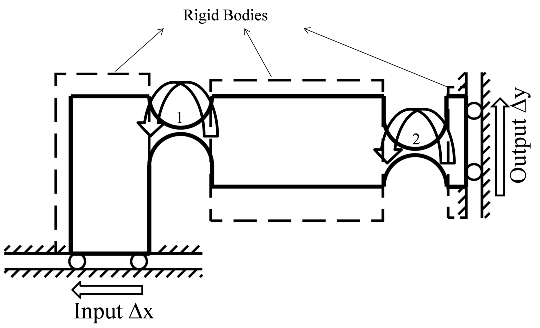

Figure 2.14: One Quarter of The Bridge Mechanism

correlate Δx and Δy and produce the amplification ratio which is $R_{amp} = \frac{\Delta y}{\Delta x}$ In order to investigate the elastic deformations of the flexure hinges and derive the amplification ratio accordingly the force coming from the piezoactoator at the highest voltage is accepted to be F_x. Having the force information the following free body diagram can be drawn in Figure 2.15 for the tilted rigid body which is between flexure-1 and flexure-2 in Figure 2.14. In Figure 2.15, once taking moment about point A and writing the static equilibrium, $(\sum M_A = 0)$ the following equation is obtained;

$$F_x l_a \sin(\alpha) - 2M_a = F_x l_a \sin(\alpha) - 2K_r \Delta\alpha = 0 \tag{2.10}$$

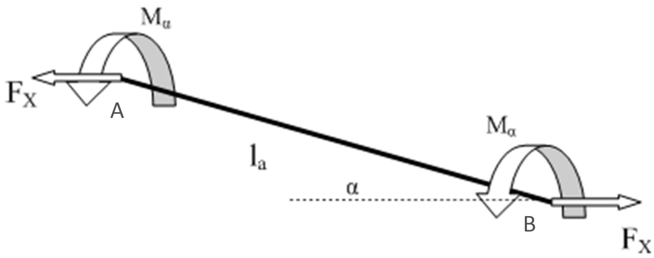

Figure 2.15: Free Body Digram of Tilted Rigid Body

In Eq(2.10) K_r is the rotational stiffness of the flexure hinge as given in Eq(2.2). Eq(2.4);

$$\Delta\alpha = \frac{F_x l \sin(\alpha)}{2K_r} \tag{2.11}$$

The force equilibrium on flexure hinge 1 in Figure 2.14 can be drawn as;

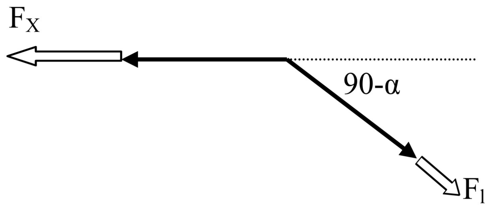

Figure 2.16: Force Equilibrium on Flexure-1

writing the static force equilibrium in Figure 2.16;

$$\frac{F_x}{\cos(\alpha)} = F_l = K_l \Delta l \tag{2.12}$$

In Eq(2.12) K_l is the longitidual stiffness of the flexure hinge as given in Eq(2.3). Rearranging Eq(2.12);

$$\Delta l = \frac{F_x}{K_l \cos(\alpha)} \tag{2.13}$$

Applying the virtual work method which can be defined as: for an arbitrary virtual displacement of a system, the combined virtual work of real forces and inertia forces must vanish [31]. Applying this phenomena to the system designed, the following relation is obtained;

$$F_x \Delta x = \frac{F_x}{\cos(\alpha)} \Delta l + 2M_\alpha \Delta\alpha \tag{2.14}$$

Putting Eq(2.11) and Eq(2.13) into the Eq(2.14) the following relation is obtained;

$$F_1 x = K_l \left(\frac{F_{1x}}{K_l \cos(\alpha)} \right)^2 + 2K_\alpha \left(\frac{F_{1x} l \sin(\alpha)}{2K_r} \right)^2 \tag{2.15}$$

From Eq(2.15) K_{in} can be obtained and be written as;

$$K_{in} = \frac{F_x}{\Delta x} = \frac{2K_r + l^2 K_l \cos(\alpha)^2 \sin(\alpha)^2}{2K_r K_l \cos(\alpha)^2} \tag{2.16}$$

From Eq(2.16) the input stiffness of the mechanism can be obtained as;

$$K_{in} = \frac{F_x}{\Delta x} = \frac{2K_r + l^2 K_l \cos{(\alpha)}^2 \sin{(\alpha)}^2}{2K_r K_l \cos{(\alpha)}^2} \tag{2.17}$$

Considering the rotation of flexures in Figure 2.14 the following equation can be written;

$$l_y = l_a \sin\alpha \tag{2.18}$$

Differentiating both sides of Eq(2.18) by considering the displacement in y direciton occurs from the rotation of flexures α, Δy can be found and written as follows;

$$\Delta y = l_a \cos\alpha\Delta\alpha \tag{2.19}$$

and using Eq(2.11);

$$\Delta y = \frac{F_x l^2 \sin(\alpha)}{2K_r} \cos(\alpha) \tag{2.20}$$

Dividing Eq(2.19) and Eq(2.16) gives the analytical amplification ratio R_{amp};

$$R_{amp} = \frac{\Delta y}{\Delta x} = \frac{\frac{F_x l^2 \sin(\alpha)}{2K_r} \cos(\alpha)}{\frac{2F_x K_r + F_x l^2 K_l \cos{(\alpha)}^2 \sin{(\alpha)}^2}{2K_r K_l \cos{(\alpha)}^2}} \tag{2.21}$$

where in the Eq(2.21) K_r and K_l values are given in Eq(2.2)-Eq(2.4). In addition, in order to find K_l, the amplification ratio is considered to be high enough to ignore Δx in R_{amp}. In a comprehensive manner, the main linear motion is accepted to rise from the motion y direction only. As a result, Eq(2.4) is used only while calculating the linear stiffness of the flexure hinges.

2.6 Optimization Procedure of Compliant Mechanism

The geometric $(l,, b, t)$ and structural (K_r, K_l) parameters which affects the amplification ratio can be seen in Eq(2.21) and in Figure 2.17. Note that the force of piezoactuator does not affect the amplification ratio in Figure 2.22. The amplification ratio is to be maximized in

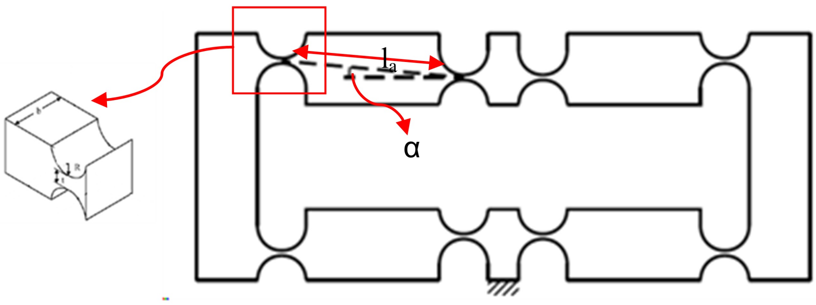

Figure 2.17: Geometric Parameters Used In Optimization

order to find the largest amplification ratio by using the parameters, R (the radius of flexure hinge), t (the thickness of flexure hinge), l_a (the length of the arm between the flexures of one quarter), α (the angle of the arm with horizontal line) and b (the thickness of overall mechanism in z direction). The mechanical constraints of the parameters are set and given in Eq(2.22) by considering the manufacturing conditions, the limitations of the empirical K_r and K_l values (0.05≤t/R≤0.65) [5]. All the constraints can be written as;

$$\begin{aligned} &2 < R < 6 \\ &0.3 < t < 1.2 \\ &3 < b < 8 \\ &3^o < \alpha < 45^o \end{aligned} \tag{2.22}$$

In addition to the geometric constraints, the stress limitations are also added to the overall optimization procedure. From Eq(2.6) the maximum bending stress that is allowed on a flexure hinge is;

$$\sigma_r = (1+\beta)^{9/20} \frac{6K_r\theta_{\max}}{t^2 b} \tag{2.23}$$

where θ_{max} is the maximum rotation of the flexure hinge and can be found from simple geometry as; $\theta_{\max} = \frac{R_{amp}A}{2l_a}$ where A is the maximum stroke of piezoactuator. Therefore the maximum allowed bending force is;

$$\sigma_r = \frac{E(1+\beta)^{9/20}}{\beta^2 f(\beta)} \theta_{\max} \tag{2.24}$$

For tensile stress using Eq(2.9) and Eq(2.17) the following equation can be written;

$$\sigma_l = \frac{AK_{in}}{bt} = \frac{A\left(2K_r + l^2 K_l \cos(\alpha)^2 \sin(\alpha)^2\right)}{2btK_r K_l \cos(\alpha)^2} \tag{2.25}$$

Directly summing the Eq(2.24) and Eq(2.25) in order to be on the safe side, the following condition condition can be formed;

$$\sigma_t + \sigma_r \leq \frac{\sigma_{allowable}}{safety\, factor} \tag{2.26}$$

In addition, since the piezoactoators are brittle materials the input stiffness of the mechanism should be lower than the piezoactuator's stiffness the following condition is to be set;

$$K_{in} < K_{pzt} \tag{2.27}$$

Note that K_{pzt} is supplied by manufacturer in APPENDIX A and given as 25 N/μm. The objective function of the optimization problem Eq(2.21) is highly nonlinear. Moreover, the structural stress constraint Eq(2.26) is another nonlinear equation in the overall optimization problem. Therefore, there is a considerable possibility to reach a local minimum in traditional optimization processes. In order solve this problem, Genetic Algorithm (GA) is selected and used. In GA, the method looks like the natural evolution encountered in nature. The 'survival of the fittest' phenomena is simulated by a fitness function being the objective function and chromosome as the variables in the objective function. The possibility of reaching local minimum is prevented in GA by crossover in each generations (runs). Crossover is a process of taking the best parents from the best solutions in each run and producing a child solution from them [32]. $MATLAB^{®}$ 'ga' built-in code is selected to perform a GA process.The details of genetic algorithm is as follows; the population size is 200, crossover fraction probability is 0.8, and total number of generations is 20. The final best individuals for the best solution is tabled as follows; Moreover, other key parameters of the mechanism can be written as fol-

Table 2.2: Optimized Parameters of The Mechanism

Type of Mechanism	Scott Russel
R_{amp}	9.21
R	3.97 mm
t	0.8 mm
b	6.6 mm
α	5.2 deg
l_a	30 mm

lows after the optimization run; the input stiffness of the mechanism is K$_{in} = 1.196N/\mu$m, the bending moment on each flexure is σ_r=36.4 MPa and the longitudinal stress on each flexure is σ_l=22.2 MPa. Superposing longitudial and bending the stresses on each flexure the stress on a flexure can be found as 58.6 MPa.

2.7 Further Key Concepts of Mechanical Design of the Mechanism

Considering the piezoactuator integration to the mechanism using the guidelines supplied by the manufacturers, the designed mechanism is updated. The supplier of piezoactoator American Piezo®provided some recommendation about the piezo mounting. As given in Figure 2.18 mounting of piezoactoator is to be performed to the given sides, the sensitive parts of the piezoactoator should not contact with the mechanism. In addition, the resulting force

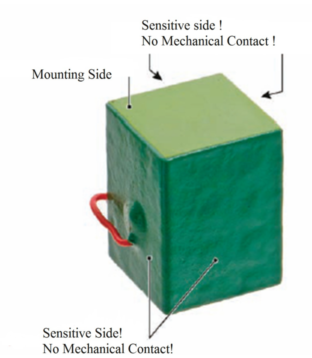

Figure 2.18: Piezoactoator Mounting Scheme-1 [30]

of the piezoactoator force vector should coincide with the mechanism axis within a virtual cylinder of $\pm 10\%$ (α angle in Figure 2.19) of actuator's cross-section to avoid excessive bending and shear stress. Moreover, coupling of piezoactoator with the mechanism is another

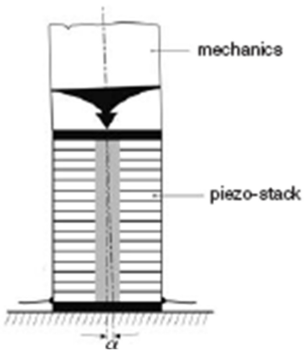

Figure 2.19: Piezoactoator Mounting Scheme-2 [30]

important issue when the mounting is considered. Plain face to plain face as in Figure 2.20 is to be avoided since even a small misalignment can lead edge squeezing with very high local pressures and ceramic failure.

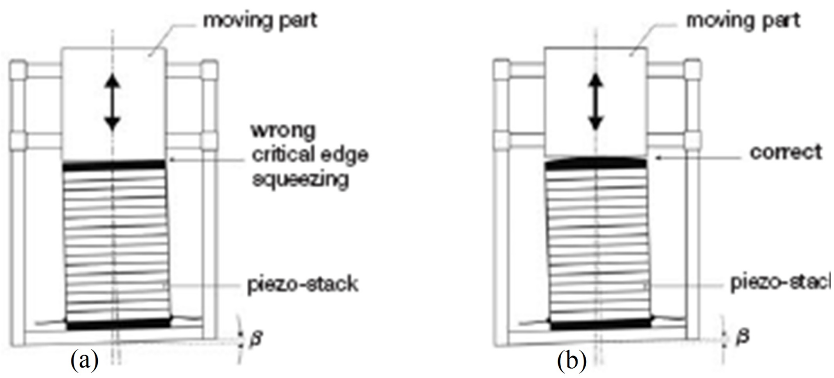

Figure 2.20: (a) Incorrect, (b) Correct Coupling of Linear Guides [30]

The maximum range of the mechanism is decided by using the piezoactuator's specifications supplied by the manufacturer. The manufacturer supplied force generation vs displacement for the American $Piezo^{©}$ Pst 150/10x10/20 which is the one used for experiments and the input stiffness of the mechanism is calculated previously as 119.6 N/μm. Plotting the graphs of two quainties gives the capacity of the overall system as follows;

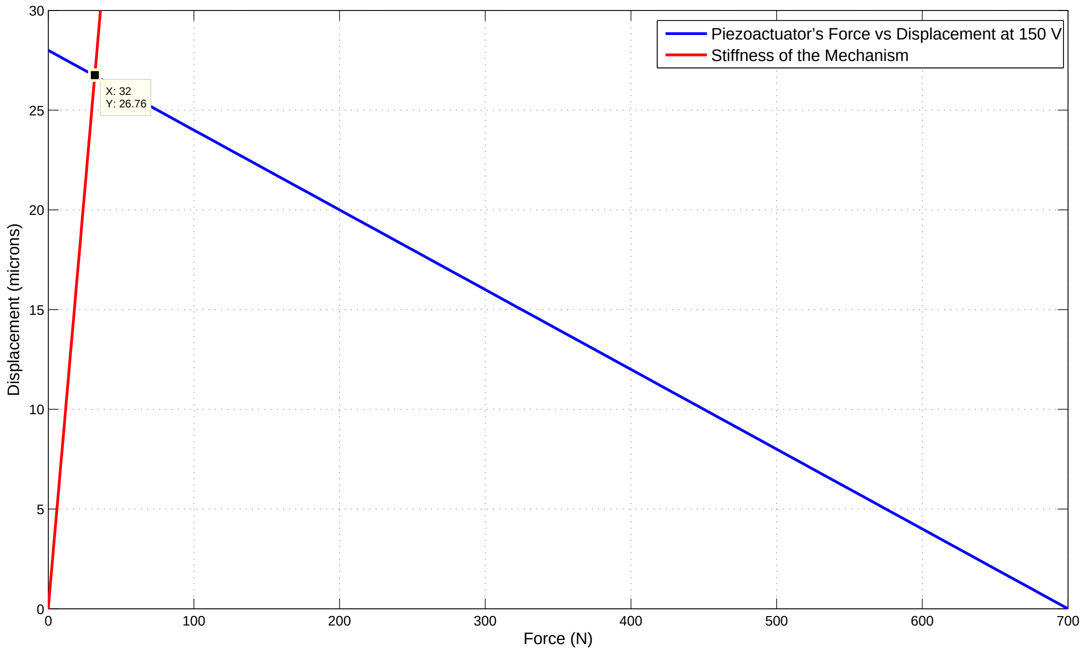

Figure 2.21: Piezo and Mechanism Stiffness Evaluation

As can be seen in Figure 2.21 the piezoactuator in the mechanism can give about 27μm output displacement and 32N output force. The displacement ratio of the mechanism reduces the output force at the same level and it will be 32/9.21=3.47N. Therefore, the mechanism designed is capable of moving a mass of $m = \frac{F}{g} = \frac{3.47}{9.81} = 354gr$ according to the analytical equations. Using the design recommendations summarized, the finalized design of the mechanism with appropriate piezoactuator mounting can be seen in Figure 2.22.

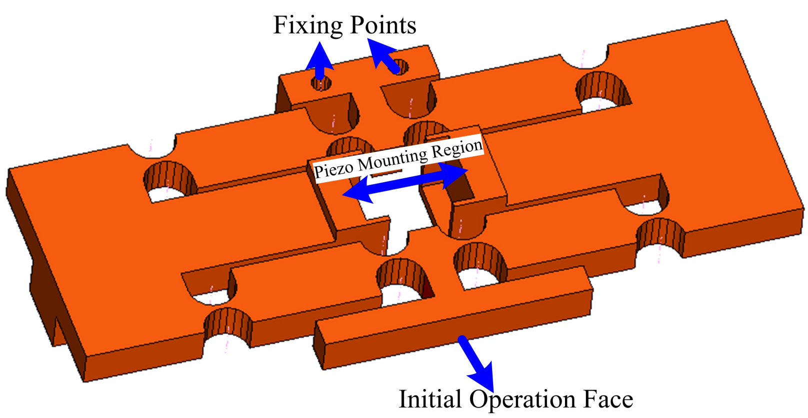

Figure 2.22: Finalized Design of the Mechanism

The initial operation face given in Figure 2.22 is to be the interface to subject to be positioned. However, for the first design which includes the mechanical design, control system design and manufacturing, the interface is just designed for the sensor readings. The final design of the mechanism is manufactured using EDM and can be seen in Figure 2.23.

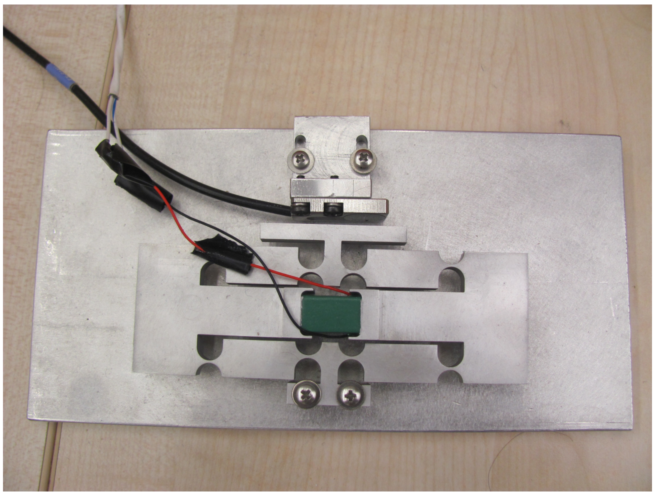

Figure 2.23: Manufactured Mechanism

2.8 Finite Element Analysis of the Mechanism

In order to validate the analytical equations derived in previous chapter, finite element analysis method is used in this work. ANSYS® gives the opportunity of analyzing the piezoelectrical effects and mechanical behavior at the same time with the help of coupled elements. Two domains of disciplines can be examined with specific mesh type such as, SOLID 227 and PLANE 13. SOLID 227 whose geometry can be seen in Figure 2.24 is a type of element that covers the three dimensional space. The element has ten nodes and able to reach five degree of freedom for each node. Coupled analysis including, structural-thermal, thermal-electric, piezoelectric etc. are available for this element [33]. Since a 3-D model is used in the analysis Solid 227 is selected and used in this study. In order to use the correct coupled analysis

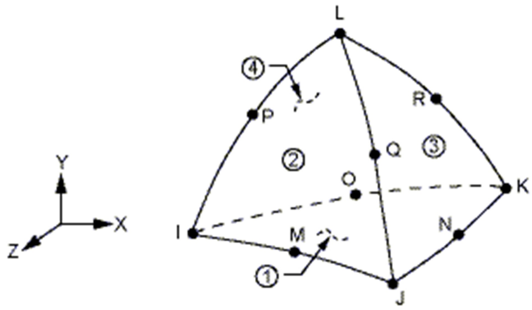

Figure 2.24: Geometry of SOLID 227 [33]

type, the correct keyoption is to be selected and for SOLID 227 the correct keyoption is 1001 to activate the piezoelectric behavior. The Eq(1.5) and Eq(1.6) can be used while modeling, however ANSYS® has a different input order than the IEEE standard on piezoelectricity [21]. In ANSYS® , the input order is (x, y, z, xy, yz, xz) whereas in IEEE standard (x, y, z, yz, xz, xy). Moreover, the suppliers give the properties of piezoactuators in IEEE standards and in order to conduct FE analysis in ANSYS® , a matrix conversion is to be performed.

After the proper conversion of the piezo matrices to a suitable form for ANSYS analysis

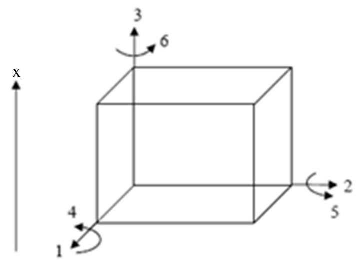

Figure 2.25: Direction of Polarization Used in FEM Analysis

and rearranging the same matrices as the main output of the piezo stack in direction x as in Figure 2.25, the elastic stiffnes matrix(the inverse of each individual element in compliance matrix), piezoelectric strain matrix and permitivity at constant electric field can be seen as follows [34];

$$c^E{}_{FEM} = \begin{bmatrix} c_{33}^E & c_{13}^E & c_{13}^E & 0 & 0 & 0 \\ c_{13}^E & c_{11}^E & c_{12}^E & 0 & 0 & 0 \\ c_{13}^E & c_{12}^E & c_{11}^E & 0 & 0 & 0 \\ 0 & 0 & 0 & c_{44}^E & 0 & 0 \\ 0 & 0 & 0 & 0 & c_{66}^E & 0 \\ 0 & 0 & 0 & 0 & 0 & c_{44}^E \end{bmatrix} \tag{2.28}$$

$$d_{FEM} = \begin{bmatrix} d_{33} & 0 & 0 \\ d_{31} & 0 & 0 \\ d_{33} & 0 & 0 \\ 0 & d_{15} & 0 \\ 0 & 0 & 0 \\ 0 & 0 & d_{15} \end{bmatrix} \tag{2.29}$$

$$\varepsilon_{FEM} = \begin{bmatrix} \varepsilon_{33}^T & 0 & 0 \\ 0 & \varepsilon_{11}^T & 0 \\ 0 & 0 & \varepsilon_{11}^T \end{bmatrix} \tag{2.30}$$

Note that in above equations, the isotrophy is taken into account. By using Eq(2.28), Eq(2.29) and Eq(2.30) and using the piezoactoator from American $Piezo^{©}$ Pst 150/10x10/20 (x) polarized properties given in APPENDIX A, a static finite element analysis in ANSYS® is performed as shown in Figure (2.26). According the supplier's recommendation, applying 120 V input to the piezoactuator, the output of the piezoactuator and the interface of the mechanism is given in Figure 2.26 and Figure 2.28.

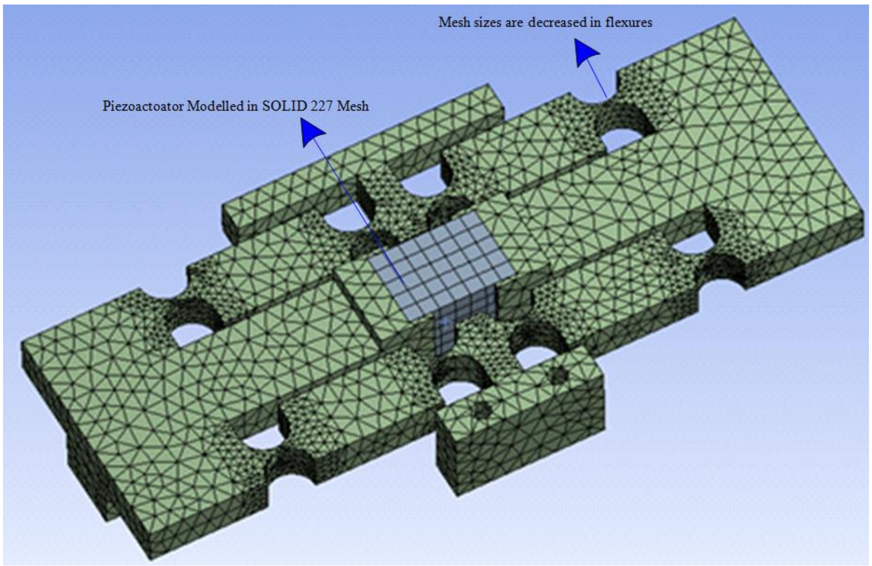

Figure 2.26: Meshed Mechanism with Piezoactuator

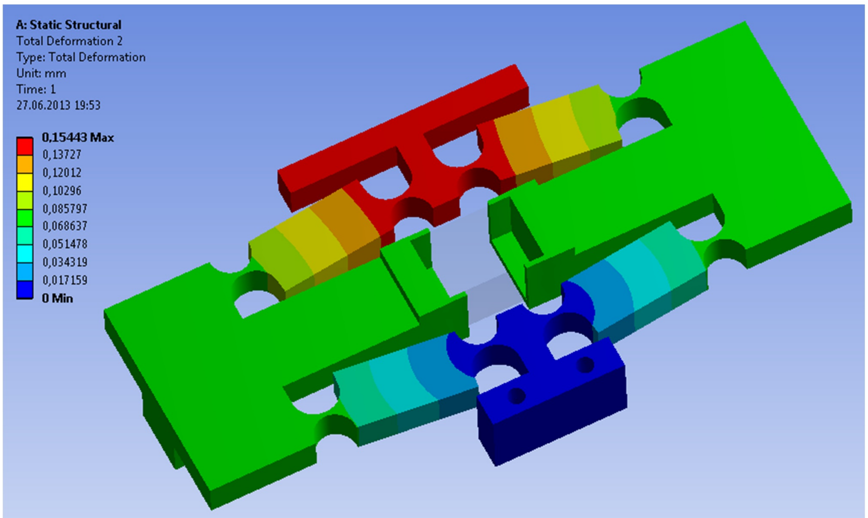

Figure 2.27: Amplified Displacement of Mechanism

By simply looking at the displacement of piezoactoator (which is 0.007853 mm in both -x and +x directions) and the displacement of the mechanism (which is 0.15443 mm in +y direction) the amplification ratio can be derived as follows;

$$R_{amp\_FEM} = \frac{0.15443}{2x0.007853} = 9.83 \tag{2.31}$$

The result of Eq(2.31) can be compared with the analytical finding. Recalling that the analytical amplification ratio is found to be 9.21 and the result coming from FEM is 9.83. The error between analytical and FEM result can be obtained as follows;

$$Error = 100x\frac{R_{amp-FEM} - R_{amp\_analytical}}{R_{amp\_analytical}} = 6.7\% \tag{2.32}$$

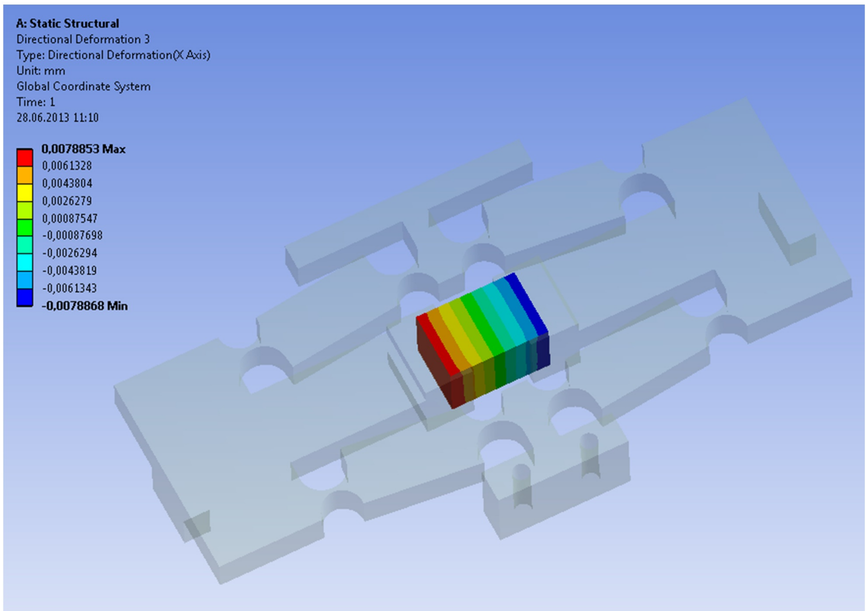

Figure 2.28: Displacement of Piezoactuator

Moreover, the stress that occurs in flexures at the maximum stroke can be investigated in FEM analysis and compared to the analytical findings. In Figure 2.29 the stress on flexure hinges can be seen; The maximum stress occurs on each flexures as can be seen in Figure 2.29 and

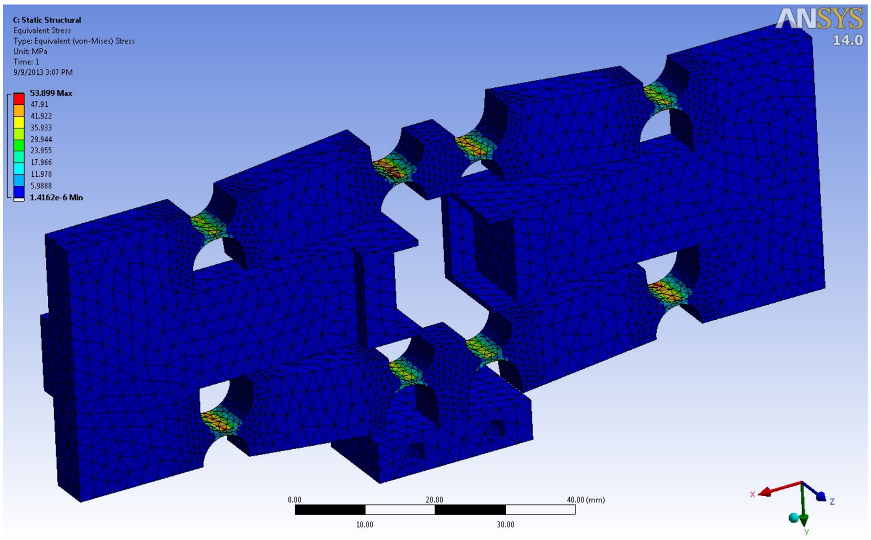

Figure 2.29: The Stresses on Flexures for Maximum Stroke in ANSYS®-1

Figure 2.30 comes out to be 59MPa from the analytical equations, in finite element analysis, however, the stress is 54MPa. The reason for this difference occurs since in analytical derivation the parts of mechanism except the flexures accepted as rigid. However, they are flexible and has a definite stiffness and absorbs the stress. Therefore, the stress on flexures declines for that reason.

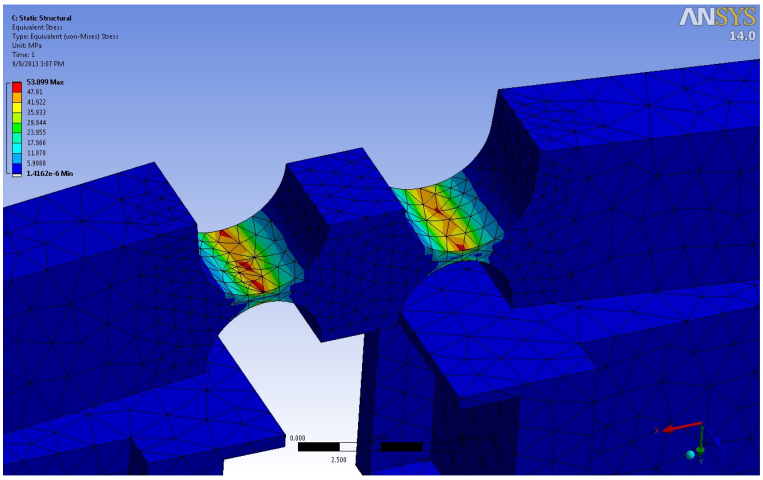

Figure 2.30: The Stresses on Flexures for Maximum Stroke in ANSYS®-2

In addition to the static analysis to find the amplification ratio, the frequency response of the system can be investigated in ANSYS® to be used for controller design for further analysis. The obtained result will be compared with the real model gathered in an experiment and the consistency of these two model will be compared and the usage of the model obtained form finite element method will be evaluated. In this manner, a harmonic sine swept test is performed (in 0-150Hz) to the system in FEM environment and corresponding frequency response of the system is plotted as in Figure 2.31.

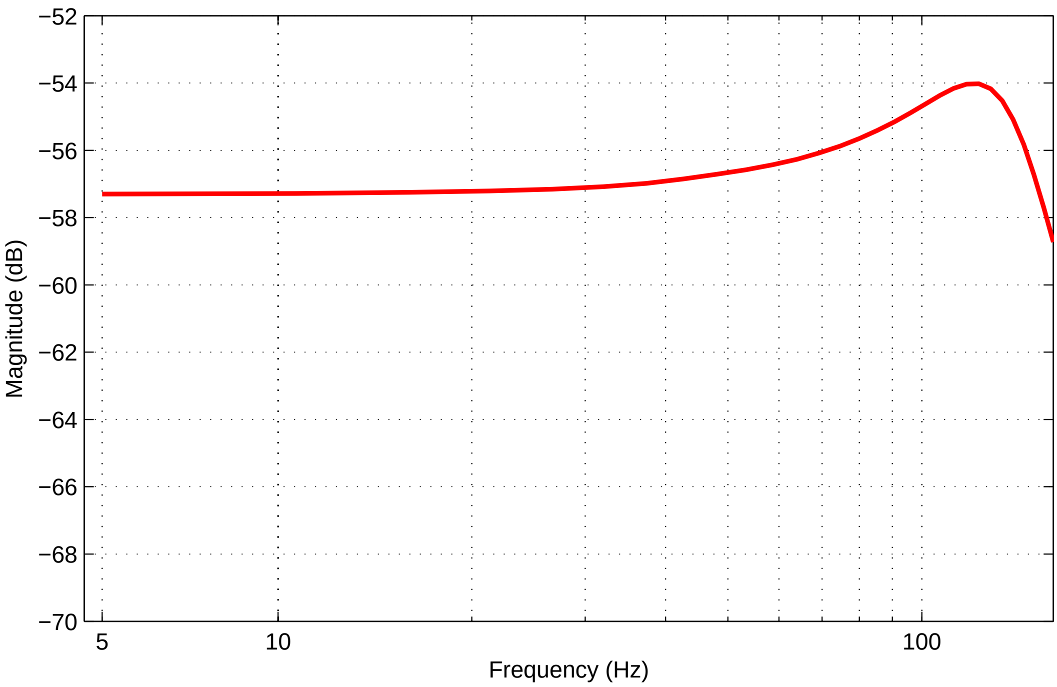

Figure 2.31: Identified FRF Using ANSYS®

CHAPTER 3

CONTROL SYSTEM DESIGN AND EXPERIMENTS

In this chapter, a control system is to be implemented on previously designed mechanism. In this way, it is aimed to compensate the hysteresis effect and reach sufficiently small steady state error. The control system design is based on the model gathered using system identification of real system. An experiment is performed both for system identification and control system testing.

3.1 Introduction

Piezoactuators exhibit hysteresis and creep behavior which could be considered as a drawback when precise positioning is of concern. Moreover, inherent structural dynamics of the designed mechanism is an additional problem for positioning. As a result of two mentioned issues, single control strategy may not be sufficient enough to get the desired performance generally [35]. In this manner, control system of the mechanism design is divided into two sections;

- Model-based feedforwad control to describe and compensate the hysteresis and creep of the piezo actuator.

- PI feedback control to get the sufficiently small steady state error of the system. The PI control system is further improved by zero phase error tracking control (ZPETC).

System identification is carried on a real experimental setup and a model is obtained for the mechanism in order to be used in controller design and validation. Following that, model-based controllers are investigated in literature and a suitable one is chosen and implemented using the model obtained in system identification. Standard PI and ZPETC controllers are added to the system using the model and all the responses to the corresponding controllers are evaluated with experiments.

3.2 System Identification Procedure and System Verification

System identification routine is performed to obtain a mathematical model of a dynamic system from measurements. In this manner, using the experimental setup in Figure 3.1 and the diagram in Figure 3.2, a logarithmic chirp signal is given to the system via Real-Time Windows Target on $MATLAB^{\circledR}$/Simulink 2010b. The reason for logarithmic chirp signal usage is covering the frequency zone (0-150Hz) logarithmically in MATLAB® in this way same scan for each frequency is succeeded. Sensor and actuator are controlled by using NI PCI-6259 DAQ Card. The voltage for piezoelectric actuator is amplified by 50 by using Pyhsik Instrumente (PI) E.413.D2 Voltage Amplifier. The voltage is sent to the piezoactuator (APC International, PSt 150/10x10/20). The displacement of the mechanism is measured by using Keyence EX-V64 digital inductive displacement sensor in millimeters.

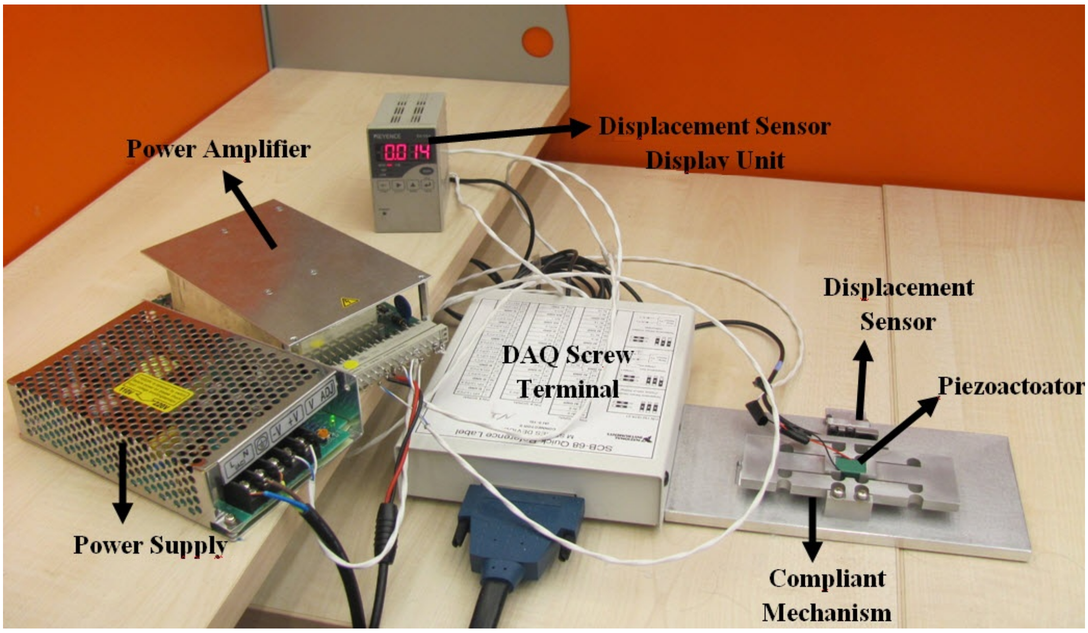

Figure 3.1: Picture of Experimental Setup

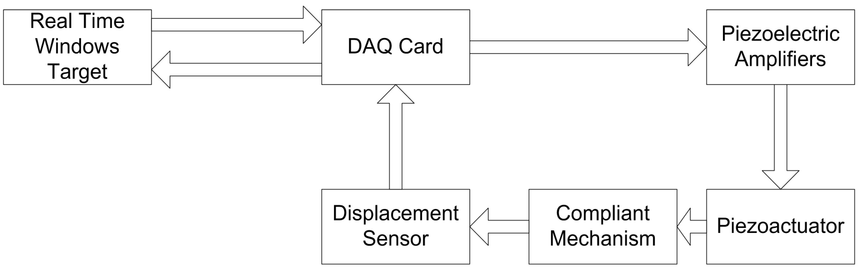

Figure 3.2: Schematic Diagram of Experiment

The logarithmic chirp signal is applied to the system for a frequency range from 1 Hz to 150 Hz for a period of 300 seconds. Piezoelectric amplifier output is used as input signal, and displacement sensor output is used as output. After collecting the displacement values from sensor, sensor transfer function is used to obtain the real displacement values. As supplied from the manufacturer, inductive sensor transfer function changes depending on the material used for measuring object as given in Figure 3.3.

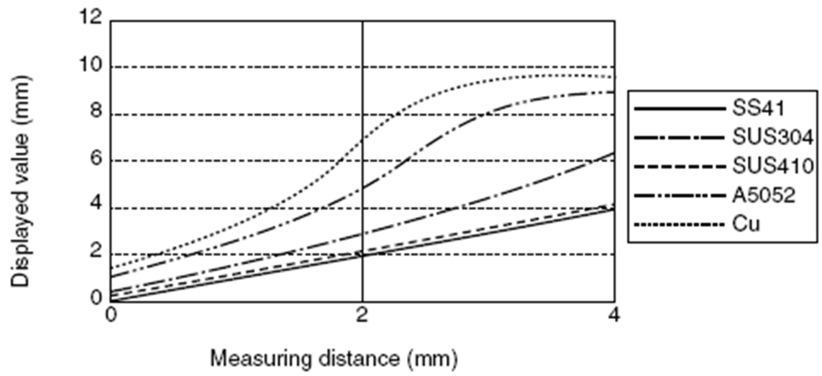

Figure 3.3: Sensor Transfer Function for Different Materials

The designed mechanism is manufactured using Aluminum 5000 series material and from Figure 3.3, the transfer function is linear for this material and it is 1.5. Adding this gain to the experimental system identification is started. Full-point FFT method is used to obtain frequency responses for better resolution. The frequency response of the system is shown in Figure 3.4;

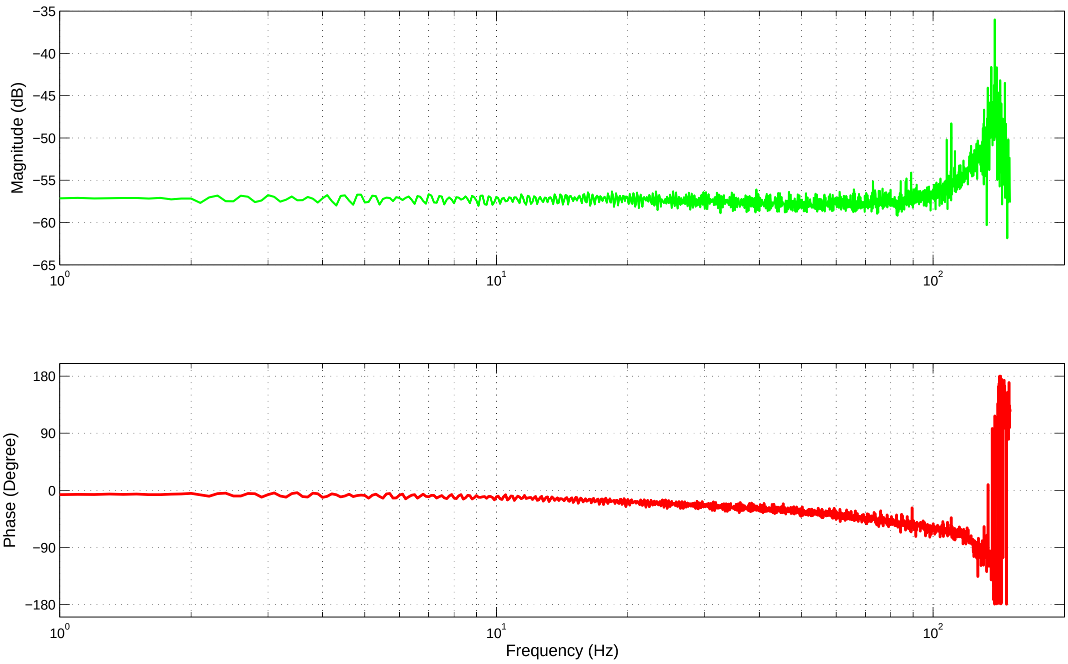

Figure 3.4: Experimental Open-Loop Frequency Response

A proper transfer function is objected to be modeled mathematically here to fit the Figure 3.4. In this manner $MATLAB^{®}$ System Identification Toolbox are used. 'pem' built-in code is used in coding with Gauss-Newton direction iterative parameter estimation method. The ‘pem’ estimates the model parameters (which can be both linear and non-linear grey-box models) using iterative prediction-error minimization method. The input to the system is given in frequency domain. The frequency weighting (which is the ’filter’ property of ’pem’ that panalizes the error with given weight in given specific frequencies) are defined as in Figure 3.5. As a result of identification, second, third and fourth order transfer functions

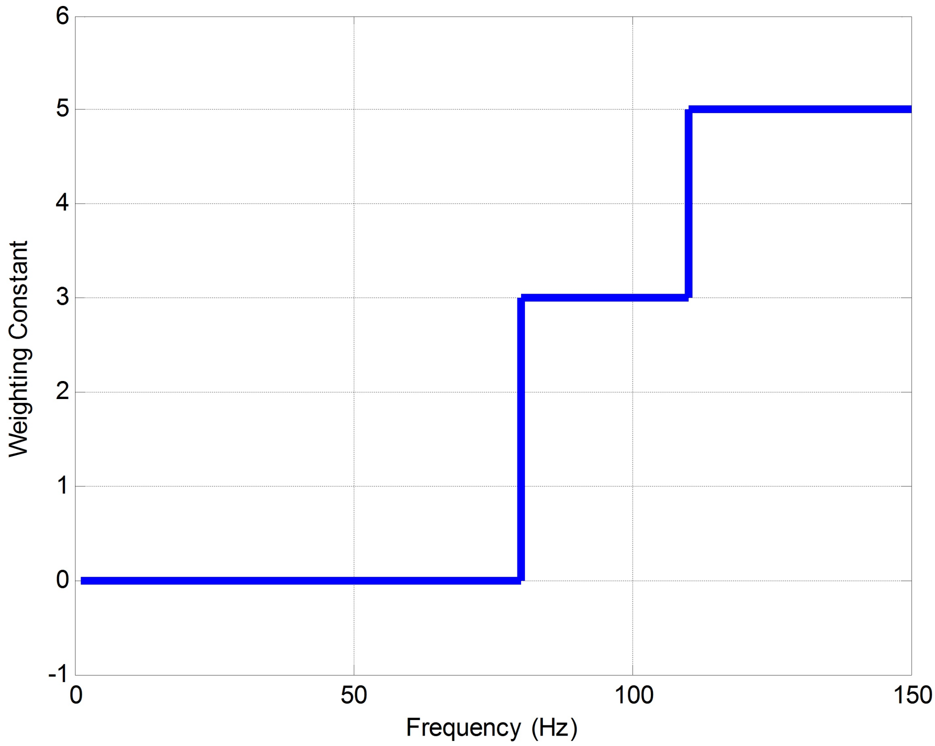

Figure 3.5: Weighting Constants Used in Modeling

are obtained. The comparison between the experimental FRF and the identified model’s FRF with different orders can be found in Figure 3.6. As can be seen in Figure 3.6 the identified model is well fitted to the experimental data with third and fourth order transfer functions. Second order transfer function with the given weighting constants in Figure 3.2 can not be fitted to the experimental response. Third order transfer function which can be seen in (3.1) is selected and used for further control system designs including feedforward modeling, PI design and ZPETC.

$$G_{open-loop} = \frac{0.39s^2 + 108.6s + 4.9 \times 10^5}{s^3 + 635.8s^2 + 7.6 \times 10^5 s + 3.4 \times 10^8} \tag{3.1}$$

The identified model can be verified to the real system by simply comparing the response of these two systems to the same input. In order to complete this task a step input of 120 V is given to the system via piezoactuator and the experimental setup explained in Figure 3.2 and Figure 3.1 .The system and model responses can be found in Figure 3.7. As can be seen in Figure 3.7, the model and the real system are compatible. In addition, the oscillations in

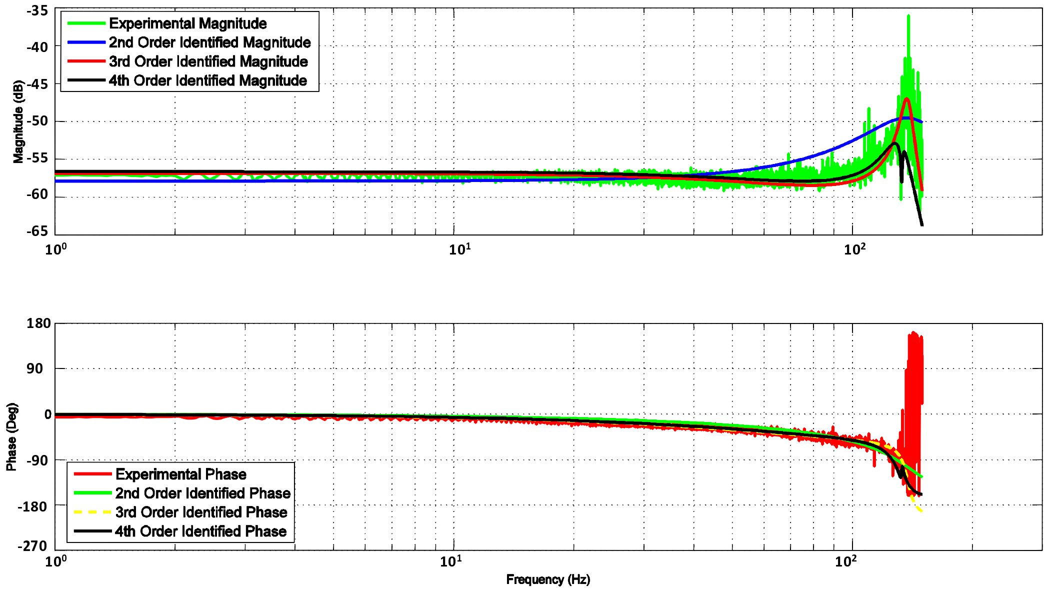

Figure 3.6: Experimental and Identified FRF's

the fitted transfer function can be seen in the figure. Note that, there is a high nonlinearity-hysteresis effect- in the experimental system which is not included to the plant modeled.

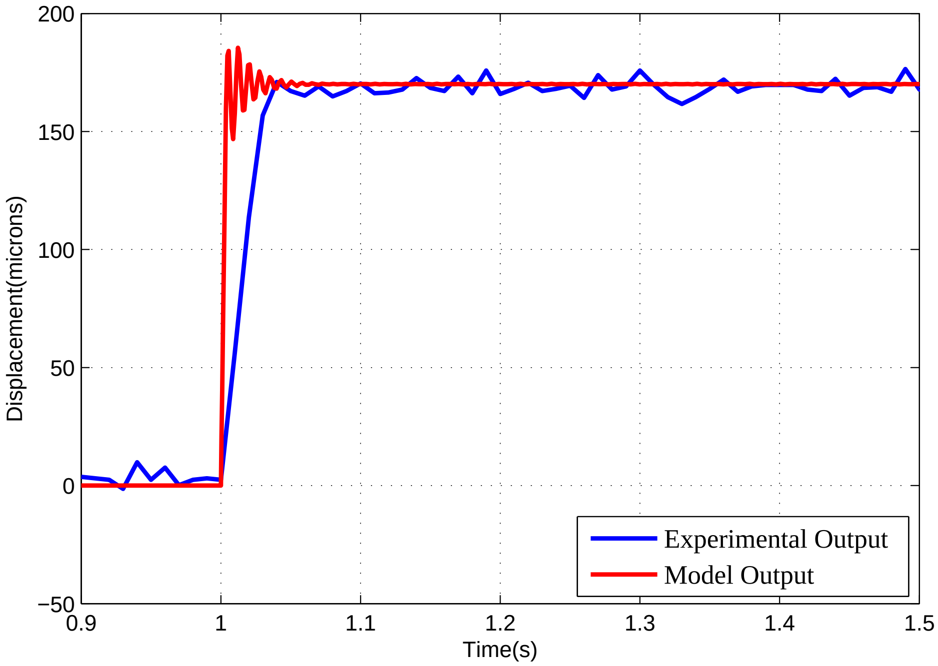

Figure 3.7: Model and Experimental Response

3.3 Model Based Feedforward Control

As mentioned before due to PZT internal dynamics, some problems including hysteresis and creep should be compensated in the system. Hysteresis is a complex input/output multi loop phenomenon affected by the existence of non local memories [36] - [37]. It can be defined as a property in which the next output depends the instantaneous value of the operation. Moreover this output dependent situation can be observed specifically at the extreme values. Many researchers have investigated this phenomenon to achieve the perfect position control and come up with different modeling techniques. Presiach [38] developed a numerical analysis approach to define the hysteresis nonlinear behavior in 1935. This solution, however, is tedious due to the fact that a pre-defined test input has to be given to the system to correlate the test inputs to the modeled system. In addition to that Presiach model does not take the frequency dependent behavior into account [39]. Maxwell [40] defined the hysteresis as a Coulomb friction on massless bodies connected to the ground with massless springs. This method is practical as it is easy to make analogy with a physical system. Implementing this method, on the other hand is a tough issue as more and more massless bodies has to be included to the system as more precision is required. Bouc [41] defined the hysteresis as a

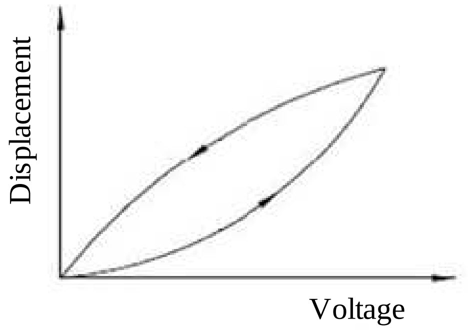

Figure 3.8: Piezoelectric Hysteresis

differential equation with particular set of parameters wihich define the shape of hysteresis. By using this method it is easy to make an analogy between a mechanical second order system and hysteresis easily by finding the corresponding parameters in the model. Bouc-Wen model is used in this work to define the hysteresis. Bouc Wen Model [42] is used experimentally to model the hysteresis of piezoelectric elements. The model is first spawned to investigate the nonlinear vibration mechanics. The variable h decides the hysteresis shape as in the follows ;

$$m\ddot{x} + b_{damp}\dot{x} + kx = F_h = k(d_{31}u - h) \tag{3.2}$$

where in the above relation m is the mass of piezoelectric actuator, b_{damp} is the damping coefficient, k is the spring coefficient, x is the displacement of the piezo actuator, F_h is the force from the piezo actuator, d_{31} is the piezoelectric coefficient that relates the voltage to displacement as given in Eq(1.5) and Eq(1.6) and h is the hysteresis coefficient. The reason for d_{31} use only in the equation sen given as in Eq(1.5) and Eq(1.6) is that, for piezostack actuators the main displacement (the highest displacement in three dimension) is in direction 3 as given in Figure 3.8. This hysteresis coefficient can be modeled as follows;

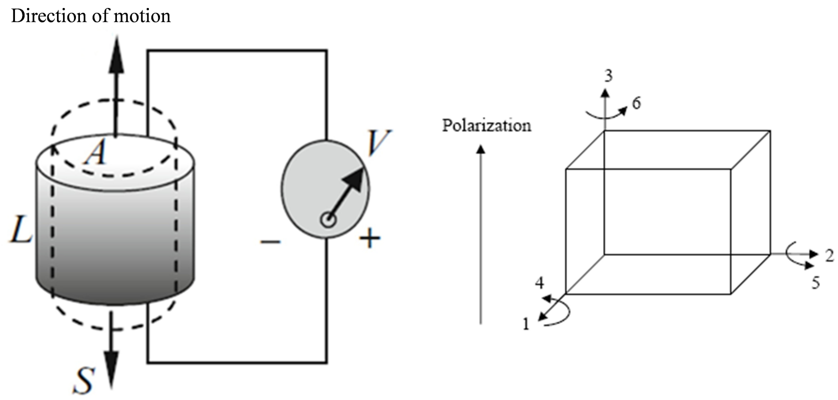

Figure 3.9: Direction of Motion for Piezostack Actuators

$$\dot{h} = \alpha d_{31}\dot{u} - \beta\left|\dot{u}\right| h - \gamma\dot{u}\left|h\right| \tag{3.3}$$

where in the above equation α, β, γ represents the parameters that forms the shape and magnitude of the hysteresis curve. The above given method is used to define the hysteresis considering the whole mechanism with the piezo actuator mounted in it. Therefore, the mass, damping and stiffness in the Eq(3.2) are not the parameters for the piezo actuator only but the whole mechanism. In order to model the system with this method and for futher control system implementations a system identification is performed.

3.4 Bouc-Wen Modeling

As explained previously, in order to compensate the hysteresis behavior of the piezoactuator, a model based technique is to be used. Bouc-Wen modeling is chosen here for this purpose. As can be seen in Eq(3.2) and Eq(3.3) the properties of the structure (stiffness, damping and mass) is needed in order to model the hysteresis with Bouc-Wen Model. In this manner, by looking at Figure 3.7, stiffness and damping of the structure can easily be found. The piezoelectric constant d_{13} of the actuator is read from the data sheet supplied by the manufacturer-which can be found in APPENDIX A. The calculated properties of the structure can be found in Table 3.1 below; By using the properties given in Table 3.1 the model can be identified.

Table 3.1: Properties of the Identified Model-2

Property	**Value**
Mass (m)	0.1 kg
Stiffness (k)	76.7 N/mm
Damping Coefficient (b_{damp})	470 N.mm/s

The method used for finding the optimum values for hysteresis operator in Eq(3.3) (α, β and

γ) an optimization procedure is to be implemented. For this purpose an initial triangle which includes a ramp input for a voltage increase and another ramp input with negative slope of the first one is to be applied to the system. The corresponding input given to the system can be seen in Figure 3.7 below. For the experimental system, the test input given in Figure 3.10 is applied and the response is recorded. The corresponding results are given below in Figure 3.11. An optimization procedure is carried on during the determination of the cor-

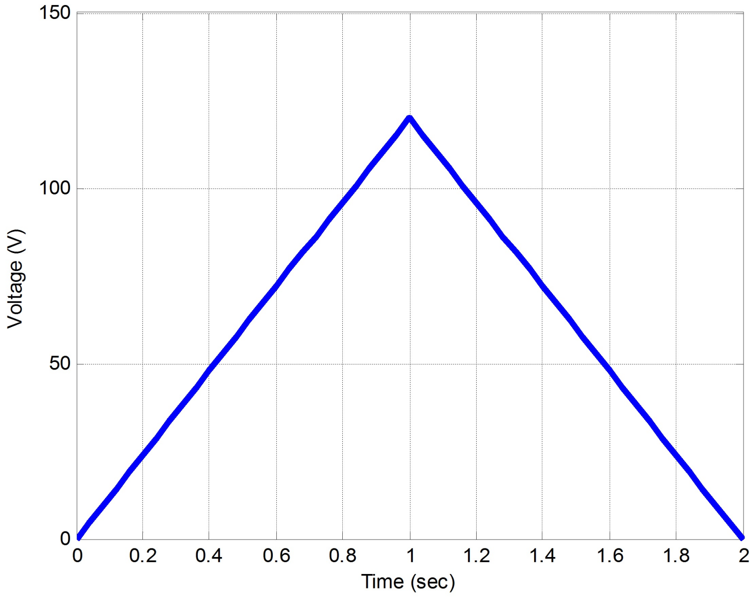

Figure 3.10: The Test Input for Bouc-Wen Model

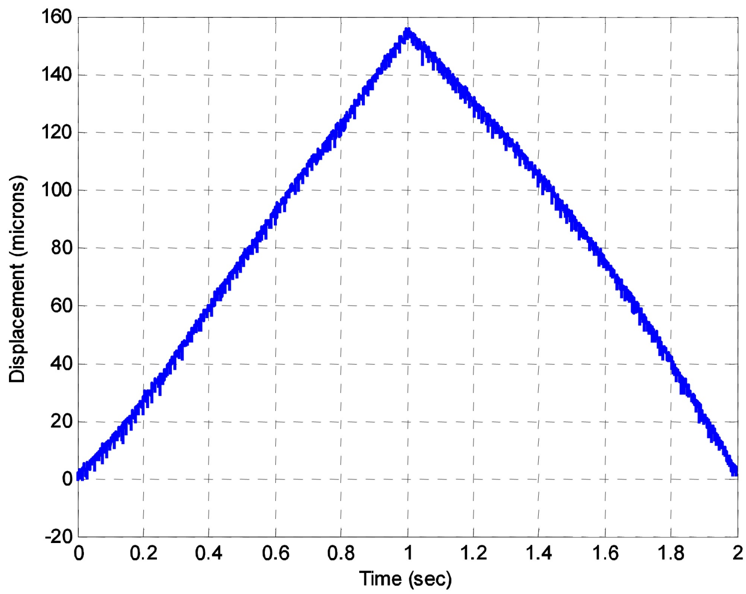

Figure 3.11: Response of The Structure to Triangle Inputs

responding hysteresis operators in Eq(3.3) (α, β and γ) to fit the Bouc-Wen model to the real response in Figure 3.12. For this purpose an objective function is to be selected in order to relate the model and experiment. As a result of this, VAF (Variance Accounting for) method which is created by Babuska [43] is chosen. In this method quality of a model is evaluated by simply comparing the standardized variance of two signals. General representation of VAF is given below;

$$VAF = 100\% \left[1 - \frac{\text{var}(y_e(i) - y_m(i))}{\text{var}(y_e(i))}\right] \tag{3.4}$$

In the above equation $y_e(i)$ represents the experimental signal whereas $y_m(i)$ is the corresponding model signal. By using Eq(3.4), the objective function can be constructed. Considering the minimization requirement, VAF percentage is substracted from 100 and final objective function is set and given below in Eq(3.5).

$$f(\alpha, \beta, \gamma) = 100 - VAF \tag{3.5}$$

For optimization $MATLAB^{®}$ Genetic Algorithm Toolbox is used. In order to get the corresponding model signals $MATLAB^{®}$ SIMULINK is used and the general view of the structure is in Figure 3.13

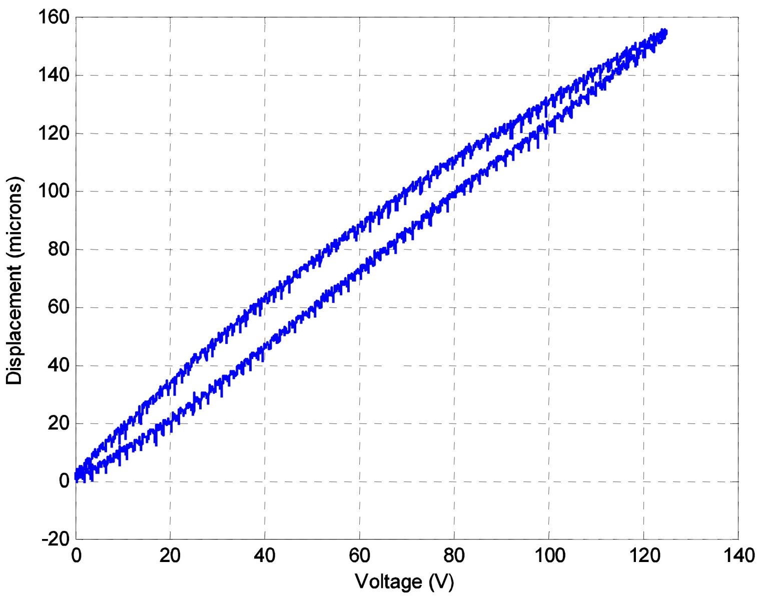

Figure 3.12: Hysteresis of The Structure

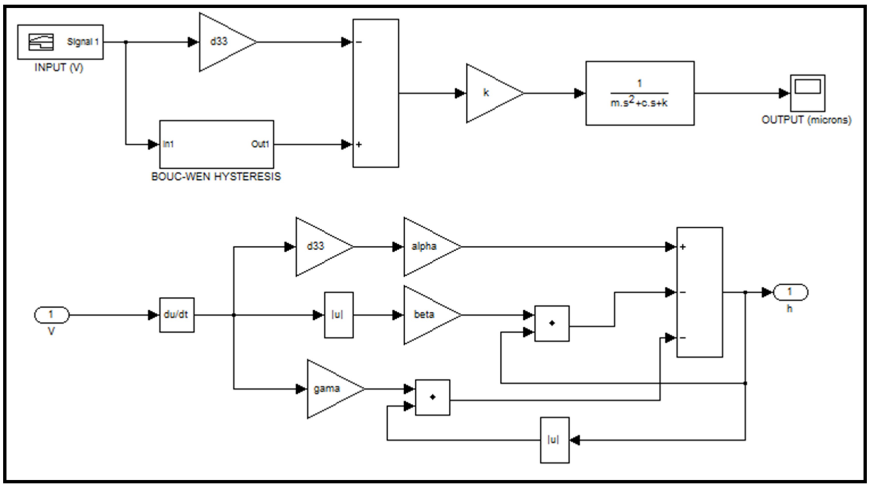

Figure 3.13: Bouc-Wen Simulink Model

The Genetic algorithm code formulation algorithm is as follows;

$$
\begin{gathered}
\text{Find} x = \begin{bmatrix} \alpha & \beta & \gamma \end{bmatrix} \\
\text{to minimize} f(x) \\
\text{subject to } -2 \leq \alpha \leq 2 \\
-2 \leq \beta \leq 2 \\
-2 \leq \gamma \leq 2
\end{gathered}
\tag{3.6}
$$

The details of genetic algorithm is decided by running some trials and decided as follows; the

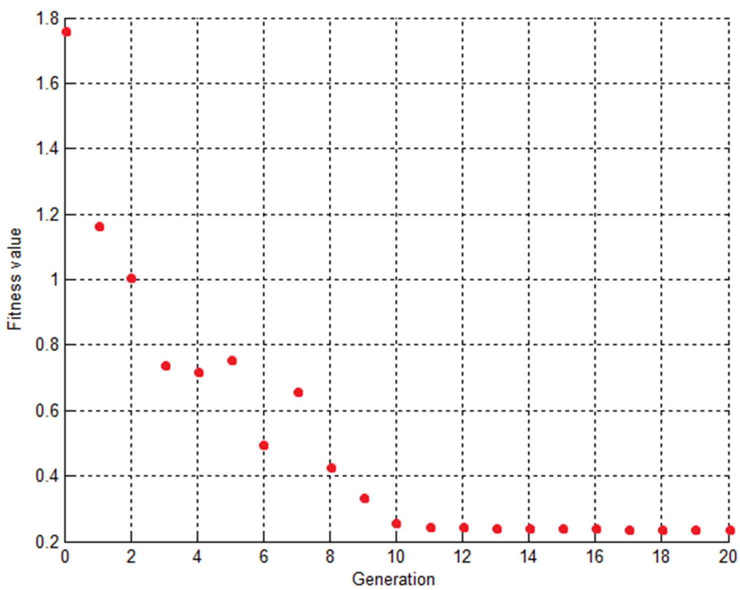

Figure 3.14: Objective Function for Each Generation

population size is 200, Crossover fraction probability is 0.8, and total number of generations is 20. The value of objective function in each generation is given in Figure 3.14.

Table 3.2: Optimized Hysteresis Operator Values

	Value
α	-1.2
β	0.02
γ	0.05

After optimization process the optimum solution set can be found in. The objective function value for the optimum values are came out to be 0.24. Therefore the VAF value for the model can be found by using Eq(3.5) as 99.76%. The optimum values of the hysteresis operators is used and the comparison of the response of the model and experiment can be found in Figure 3.15 and Figure 3.16.

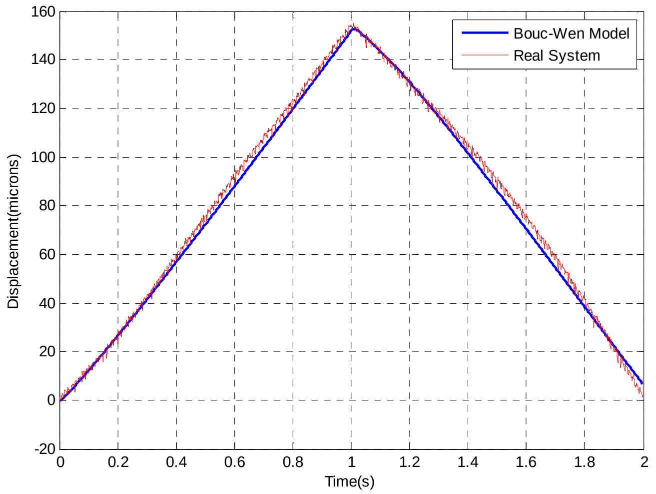

Figure 3.15: Response of the Structure and Model to Triangle Input

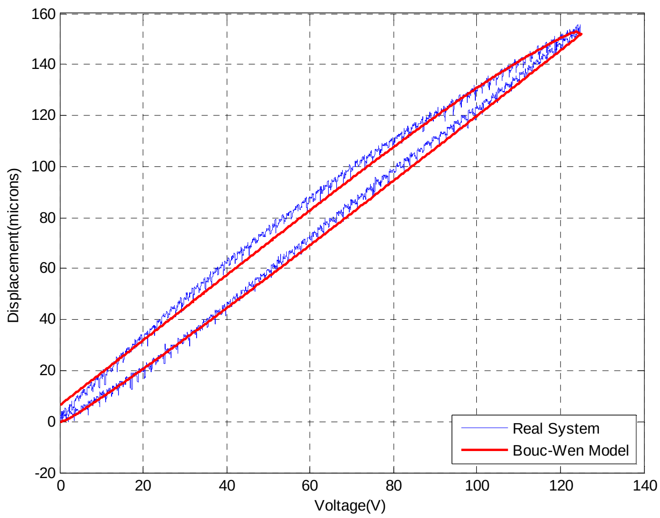

Figure 3.16: Hysteresis of the Structure and Model

3.5 Feedback Controller Design

The open loop transfer function is obtained in previous sections. A proper PI controller is to be designed and added to the system and its performance is to be observed and evaluated for final system. In this manner, by using the open loop transfer function in Eq(3.1) a PI controller system is designed via $MATLAB^{®}$ SISOTOOL. The method used in designing the controller is Ziegler-Nichols step response which approximates the plant as a first order model with a time delay and computes the PI parameters using classical process reaction method of Ziegler-Nichols. The hysteresis nonlinear behavior of the system is ignored and the system is accepted as a third order linear system with two zeros. The PI controller is chosen for feedback control due to the fact that the steady state error is needed to be as low as possible and there is no requirement for the speed of the system and there is plenty of noise coming from the displacement sensor so derivative controller is not included. For the open-loop plant the following design requirements are given to the toolbox. Rise time is 0.04 seconds, settling time is 0.08seconds, and percent overshoot is 20% . The general view of the closed loop system response to a unity step input is shown in Figure 3.17. The designed PI

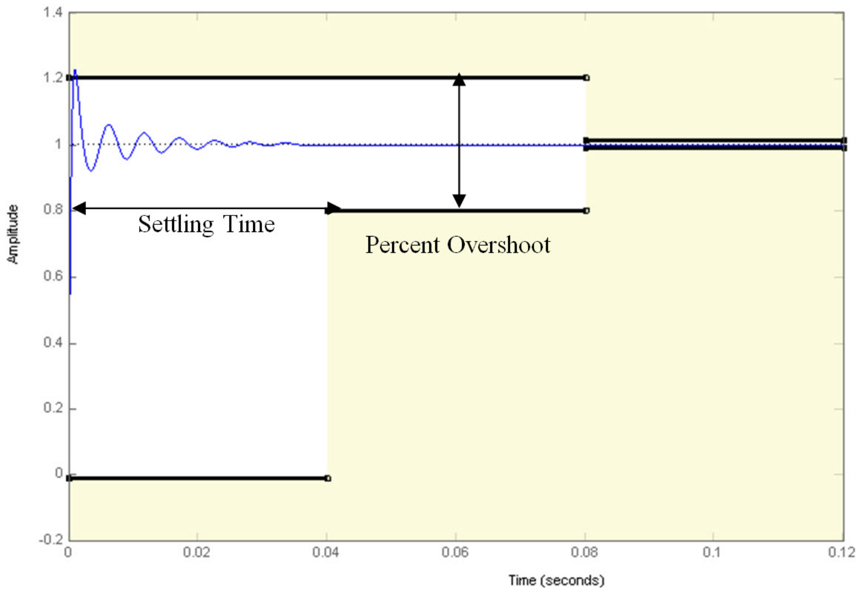

Figure 3.17: Closed-Loop Response in SISOTOOL

controller is given in Eq(3.7);

$$G_c = 8721(1 + \frac{2009}{s}) \tag{3.7}$$

By simply looking at the Eq(3.7) the controller parametes can be written as;

$$\begin{aligned} K_p &= 8721 \\ K_I &= 2009 \end{aligned} \tag{3.8}$$

3.6 Zero Phase Error Tracking Control (ZPETC) System Design

In previous sections, two control algorithms are designed. Their effects on real system is to be evaluated afterwards in the following sections, In this section, one alternative control algorithm is to be designed and implemented to the system. The effects of three different control algorithms is to be examined. The main purpose here is to finalize the overall control system with the best combination and use it in final design. In this sense, Zero Phase Error Control System is designed and applied to the system.

Tomizuka [44] proposed a feedforward control method which eliminates all the poles and zeros and most importantly phase error of a servo system. In this method it is possible to track a reference input more precisely. The general view of the proposed feedforward control system as in Figure 3.18 The theory behind this method is to eliminate the error that sticks in

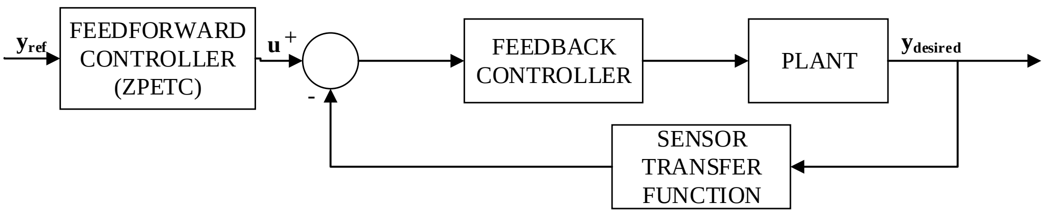

Figure 3.18: General View of ZPETC Feedforward Control

the inside of the servo system. The reference signal is reshaped by the feedforward and more care is taken onto frequency components of the real system. A closed loop transfer function without a feedforward control can be written as in discrete time domain as below;

$$G_{cl}(z^{-1}) = \frac{z^{-d}B_c(z^{-1})}{A_c(z^{-1})} \tag{3.9}$$

$$\begin{aligned} A_c(z^{-1}) &= 1 + a_1 z^{-1} + a_2 z^{-2} + \ldots + a_{n_a} z^{-n_a} \\ B_c(z^{-1}) &= b_0 + b_1 z^{-1} + b_2 z^{-2} + \ldots + b_{n_b} z^{-n_b} \end{aligned} \tag{3.10}$$

where $n_a \leq n_b$ and d is the time delay. The numerator of the Eq(3.9) can be divided into two. First one as the zeros that is outside or on the unity circle and second the zeros that are inside the unity circle as below;

$$B_c(z^{-1}) = B_c^+(z^{-1}) B_c^-(z^{-1}) \tag{3.11}$$

where $B_c^+(z^{-1})$ represents the roots outside the unity circle (non-minimum phase factors) and $B_c^-(z^{-1})$ represents the roots inside the unity circle (minimum phase factors). By using the Eq(3.9), Eq(3.10) and Eq(3.11) Tomizuka divided the feedforward control in Figure 3.18 into three sub-elements as in Figure 3.19.

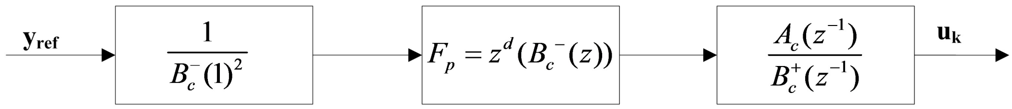

Figure 3.19: Sub-Elements of Feedforward Control (ZPETC)

The identified model of the mechanism and the corresponding PI transfer function designed can be written in closed loop transfer function in discrete time domain as follows;

$$G_{cl} = \frac{-0.12z^{-4} + 0.2686z^{-3} - 0.0305z^{-2} - 0.2683z^{-1} + 0.1509}{0.6768z^{-4} - 2.965z^{-3} + 4.895z^{-2} - 3.606z^{-1} + 1} \tag{3.12}$$

The sample time of the above equation is 0.0001s. By using $MATLAB^{®}$ feedforward control in Figure 3.18 is designed and given in APPENDIX B as follows;

$$G_{zpetc} = \frac{0.677z^{-4} + 2.965z^{-3} + 4.891z^{-2} - 3.606z^{-1} + 1}{-0.796z^{-4} + 1.781z^{-3} - 0.202z^{-2} - 1.779z^{-4} + 1} \tag{3.13}$$

The Bode plots of the feedforward control(ZPETC) only, PI controlled closed loop of the system and the overall system given below shows the phase and magnitude of the overall system remains as 0dB in Figure 3.20 which means the system will track any input given.

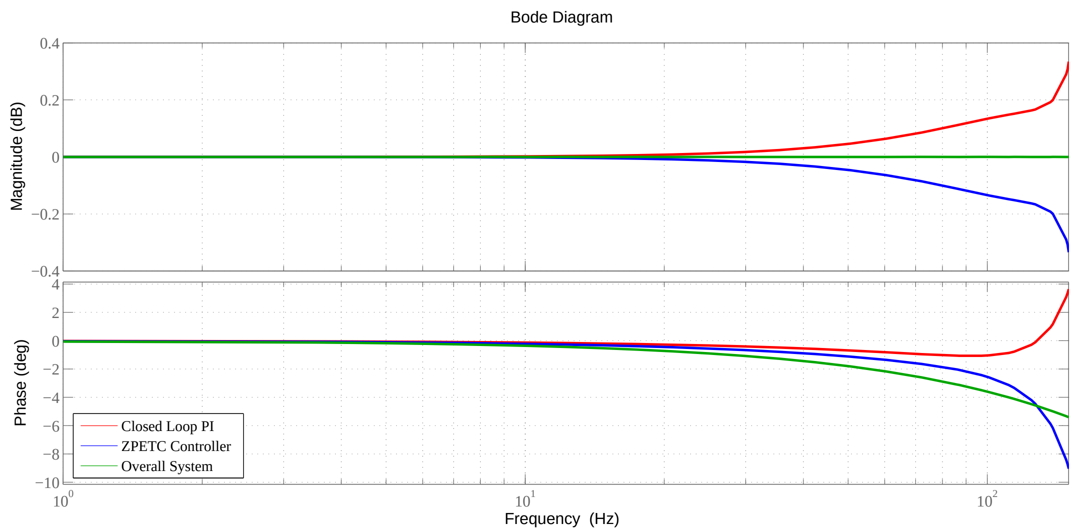

Figure 3.20: Bode Plots of the System and Controllers (Effect of ZPETC)

3.7 Model and Experimental Verification

In this part of the study the designed controllers and models constructed will be tested and compared with the real system. In order to complete this task. A positioning scenario is to be created. A reference input as in Figure 3.21 is selected as the scenario. The sharp corners are chosen specifically to test the performance of the controllers and model in a tough duty.

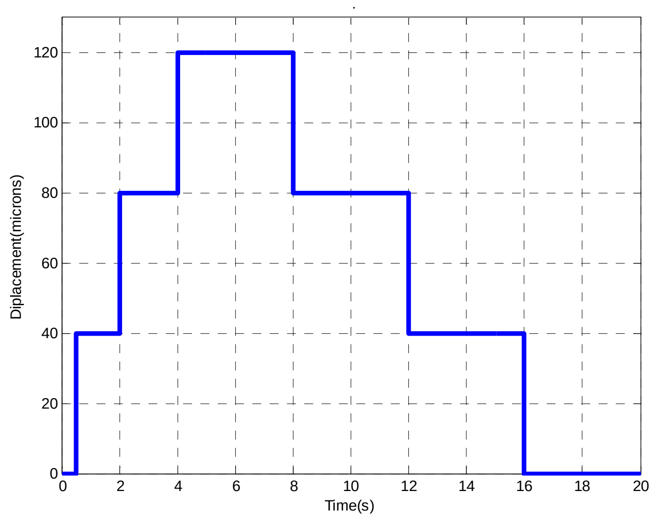

Figure 3.21: Reference Input to Track

The SIMULINK block system used for each different control algorithm is given in figures below;

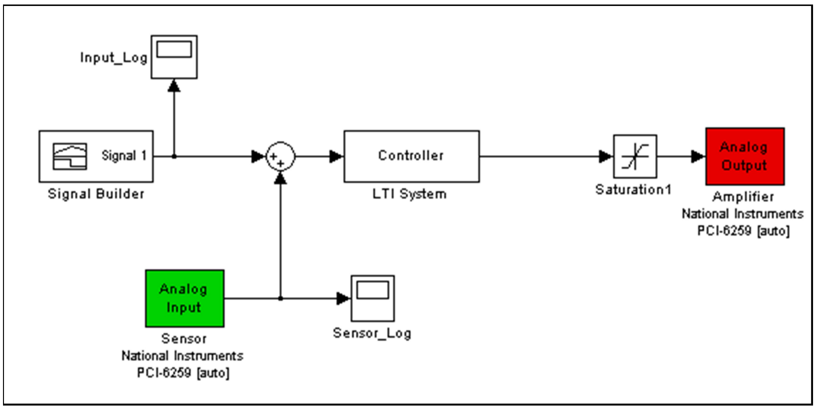

Figure 3.22: PI Controller Used in Experiment

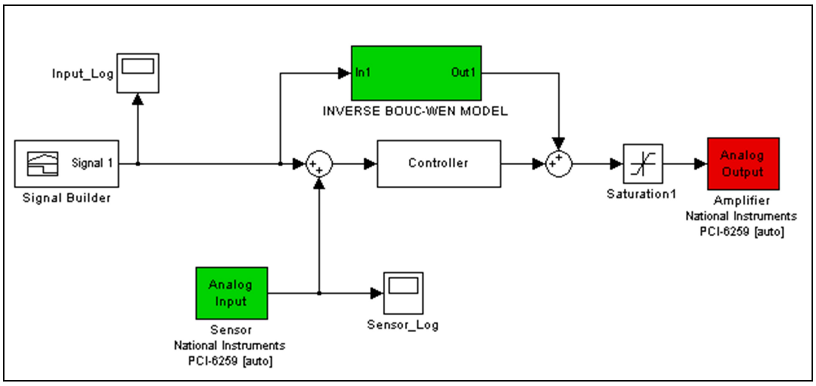

Figure 3.23: PI+FEEDFORWARD (BOUC-WEN) Model Used in Experiments

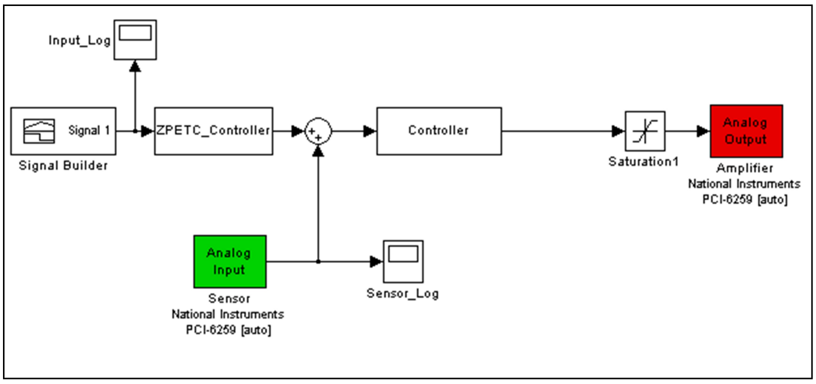

Figure 3.24: PI+ZPETC Controller Used in Experiments

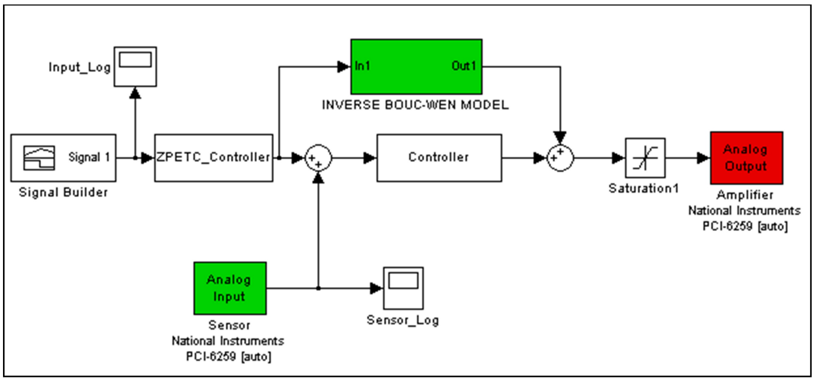

Figure 3.25: PI+ZPETC+FEEDFORWARD Model Used in Experiments

The performance of the controllers designed beforehand can be found in Figure 3.26 Looking

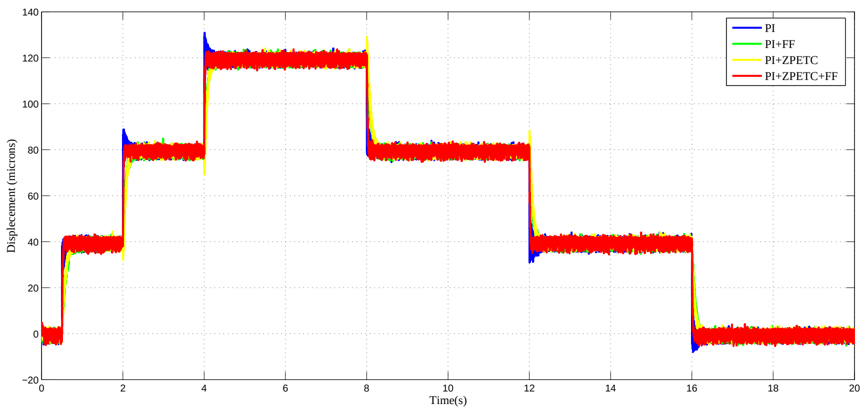

Figure 3.26: Controller Performance Comparison-1

at the Figure 3.26 more closely (between 4th and 5th seconds) in the Figure 3.27, It can be seen that the PI controller only makes the system oscillate while converging the desired position. In addition, the errors for each controller can be seen in Figure 3.28 Feedforward and/or ZPETC control gives the system settle as an overdamped system and more quickly. This is due to additional poles and zeros to the system which cancels the complex conjugate pair poles. In addition, it is very obvious that if ZPETC and Feedforward controls used together

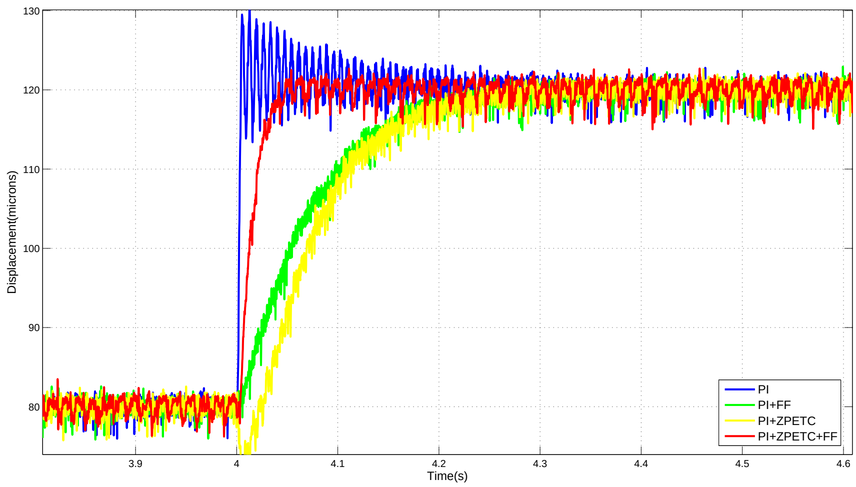

Figure 3.27: Controller Performance Comparison (Closer View)

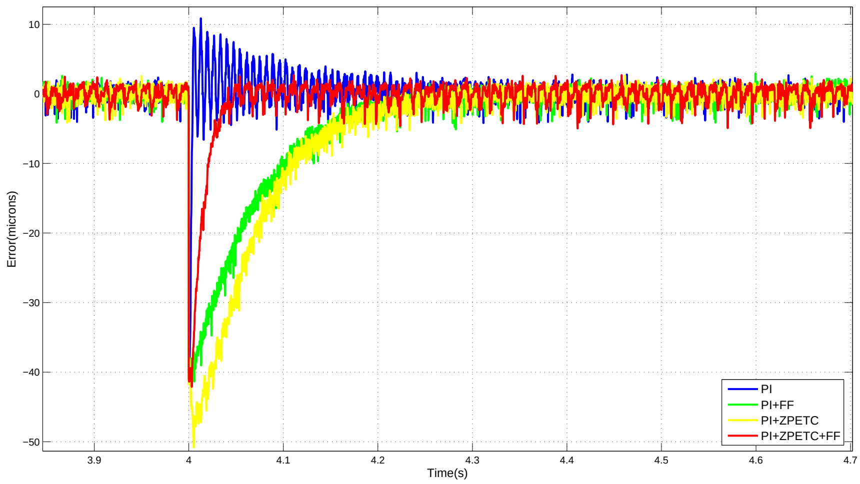

Figure 3.28: Error Comparison for Different Controllers

as an addition to PI controller the system settles the quickest. However, the steady state error of all different control algorithms seem to be the same, the insufficent sensor resoluion can be given the reason for this issue. In order to see the steady state error performance of the controllers the sensor resolution can be further improved. By using the Eq(3.4) the numerical comparison data can be acquired and in addition to the graphical identification an analytical identification can be done for deciding the which controller should be used. In Table 3.3 the VAF values of the controller performance compared to the reference input can be found. The reference input is used as the experimental signal and the systems output for each different control algorithm is used as the model output here. The controller performance is also tested with a sine input in order to be able to see the hysteresis behavior of the overall system since the displacement command increases and decreases in a definite frequency in sine input and in this way the hysteresis behavior is more clear. The response of each controller to a sine input of 1 Hz and an amplitude of 150 microns is recorded for each controller and given in Figure 3.29 and in detail in Figure 3.30.

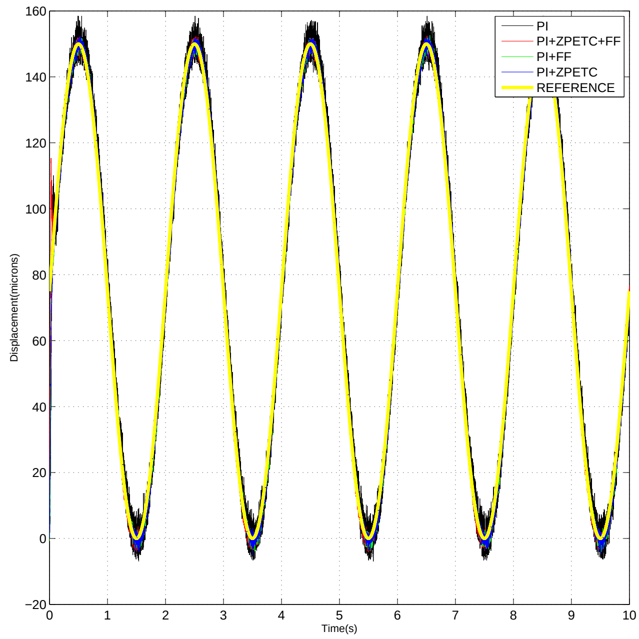

Figure 3.29: Sinusoidal Trajectory Tracking of Different Control Algorithms-1

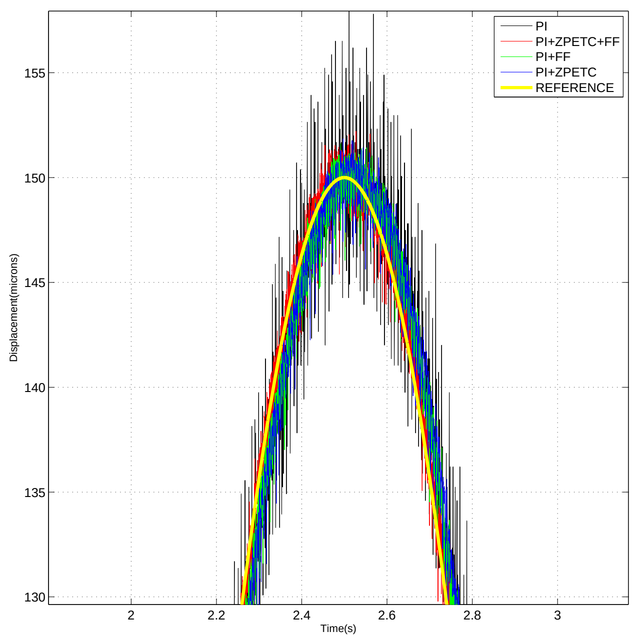

Figure 3.30: Sinusoidal Trajectory Tracking of Different Control Algorithms-2

Table 3.3: VAF Values for Different Controllers

Controller Type	VAF%
PI	99.64%
PI+FF	99.85%
PI+ZPETC	99.72%
PI+FF+ZPETC	99.92%

The corresponding errors for the input above can be seen in Figure 3.31;

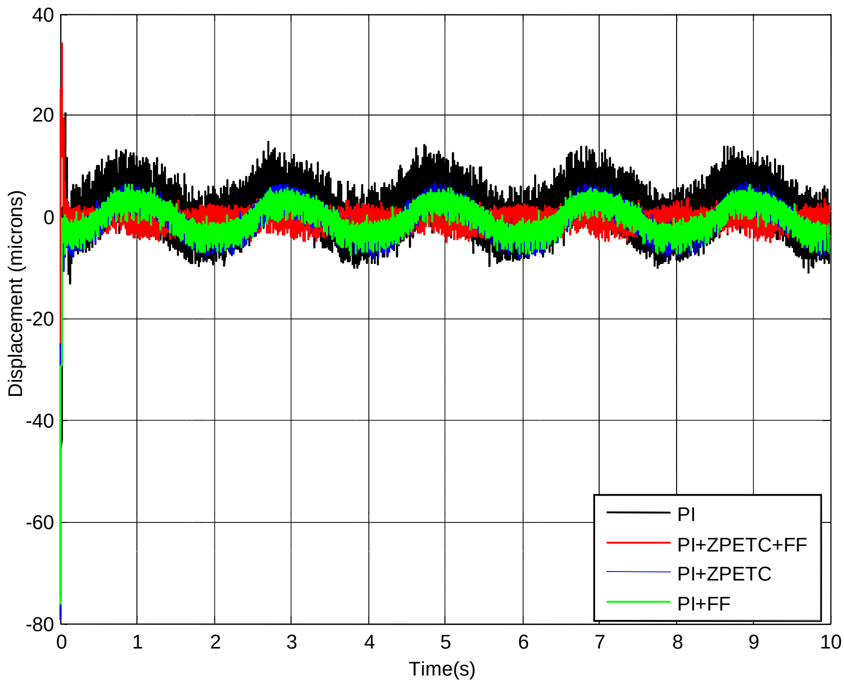

Figure 3.31: Error Comparison for Sine Tracking

As can be seen in Figure 3.31 only PI controller is not satisfactory for the desired steady state performance due to hysteresis effect, however a feedforward controller design or ZPETC design reduces the error and together usage of these two controllers gives the best result. Moreover VAF values for the sine input given is calculated for all control algorithms and can be found in Table 3.4.

Table 3.4: VAF Values for Different Controllers-2

Controller Type	**VAF%**
PI	96.64%
PI+FF	99.35%
PI+ZPETC	98.32%
PI+FF+ZPETC	99.89%

3.8 Design Verification

During design process some basic design tools which include the finite element modeling, analytical modeling and experiments are conducted. In this part of the study all the findings are compared and the general approach to the design is validated. In this way, it is aimed to obtain a design guide for furher positioning mechanism designs. First of all, the amplification ratio derivation is compared both from analytical, finite element and experimental finding. From Figure 3.16 and Figure 3.17, an input of 150 V to the piezoactoator makes the mechanism to move 153 microns and from the piezoactoator supplier the expected output of the actuator itself at this voltage is approximately 15.5 microns. Therefore the amplification ratio of the real system is 9.87; Recalling from Eq(2.31) the amplification ratio is found as 9.83 from finite element analysis and from analytical findings the ratio is 9.21. Accepting the real system as the true value for amplification ratio, the deviation from this value for analytical and finite element calculations can be found in Table 3.5.

Table 3.5: Percentage Errors for R_{amp}

	R_{amp}	**Error%**
Experiment	9.87	-
FEM	9.83	0.4%
Analytical	9.21	6.7%

As can be seen from Table 3.5 the finite element method fits very well to the experiments and analytical method is also fits good to experimental findings. Therefore for a new design procedure both analytical and FEM methods can be trusted. In addition to amplification ratio the frequency response of three methods are compared and given in Figure 3.32.

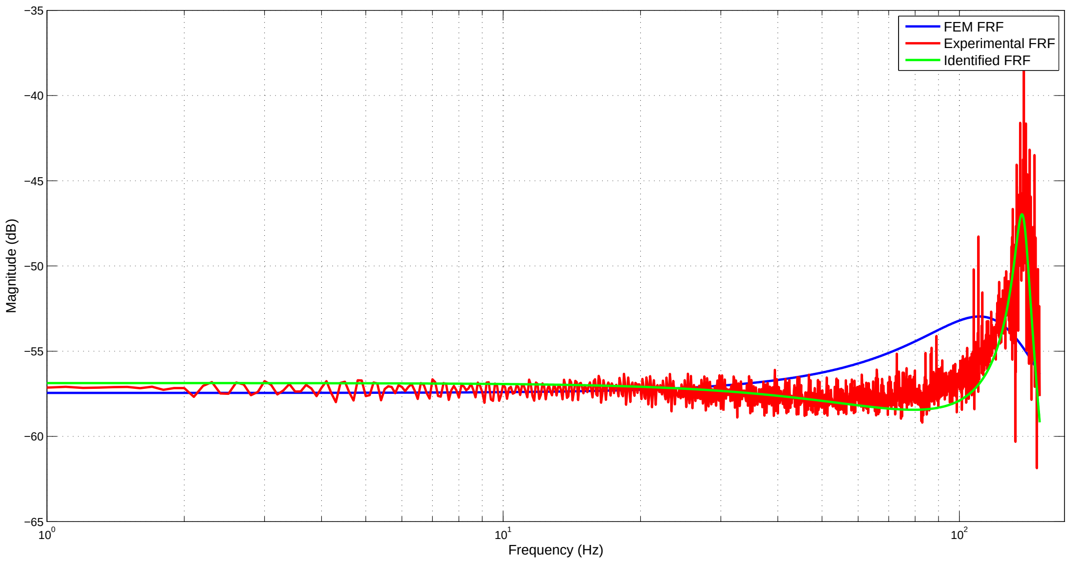

Figure 3.32: Experimental Analytical and FEM FRF Comparison

From Figure 3.32 the frequency response found from finite element method differs from the other two frequency reponses (experimental and model obtained from system identification). The reason for this error is the damping ratio. In $ANSYS^{®}$ only the structural damping is allowed to be used and even in electromechanical elements which gives opportunity to couple electrical and mechanical interfaces the hysteresis damping option is not available. Therefore, since damping is not entered correctly (the supplier's given properties are not exact values) the damping controlled region in Figure 3.32 is not fitted the two other plots. The remaining parts (the parts except the damping controlled region- the natural frequency zone) are well fitted to the other two graphs.

3.9 Conclusions

For the designed compliant mechanism with piezoactuator mounted, various controller strategies are applied. The conventional PI feedback controller is the main controller that is included to the system to control the system by using the error. However, since there exists nonlinearity in the system due to the existence of the piezo, this phenomena should also be taken into account. The method used to succeed this was using a feedforwad model called Bouc-Wen model. This model with a PI controller gives the desired result. In addition, Zero Phase Tracking (ZPETC) Controller is used to eliminate the modeling error during system identification and PI control design and to see the effect on the nonlinear behavior of the system. The results is satisfactory too. As a result, for this kind of a system in order to control the system with about 3-4 microns steady state error, the selected controller is PI+ZPETC for the designed system since ZPETC has an advantage of easy modeling when compared to Bouc-Wen model. Bouc-Wen model requires more mathematical work. The further performance comparison of these controllers can be examined with more improved displacement sensor which may change the controller performances and the selection can also be changed accordingly. More detailed performance comparison of different control algorithms can be implemented in this way.

CHAPTER 4

SUMMARY CONCLUSIONS AND FUTURE WORK

4.1 Summary

In this study a general approach to design, modeling and control of a single axis precise position control of a compliant mechanism driven by a piezoactuator is given. The main aim of the study is to develop a precise positioning mechanism to be used both in dynamic tracking and alignment purposes. In this manner, in the first part of the work, the motivation of the study is given with examples from literature and market. The possible problems are defined and their common solutions are summerized. After problem definition, the objective of the study is explained and the answer to the question "how the problem can be solved?" is given. Afterwards, some basic concepts and backround information about the problem is explained both for the mechanism alternatives and piezoactuator concepts. Following that, the examples from literature are examined and given in detail. The previous works found in literature (both about the compliant mechanisms and precise positioning) are investigated and some comments on them are given. In second chapter, the mechanical design point of view is investigated. In order to decide an appropriate mechanism, a comparison matrix analysis is performed with five candidates and the best mechanism is selected among them. After selecting the mechanism type, the mechanism is modeled using "pseudo rigid body model" to find the maximum possible amplification ratio. In addition, the piezoactuator mounting consideration while designing the mechanism is also examined and explained. After completing the design, the parameters are compared with finite element method and verified. The final mechanism is manufactured using EDM (Electro Discharge Machining). Third part of the study includes the control system design and experiments, model based control (Bouc-Wen Mode) and Zero Phase Error Tracking Control (ZPETC) concepts are introduced and designed. System identification procedure is complated using an experimental setup. Following that, the designed control algorithms are tested on the same setup and their performances are compared and evaluated. The main aim of this chapter is to obtain a design guide for such precise positioning mechanisms.

4.2 Conclusions

Considering the results obtained in previous chapters the following conclusions could be made;

- Among the possible mechanism configurations the bridge type mechanism is chosen with a proper weighting which is constructed according to the requirements of the work which is decided in first chapter.

- General analytical equations about the amplification ratio are driven (for a bridge type mechanism) from analytical equations using pseudo rigid body model and the derived equations are proven with both finite element methods and experiments with about 7% deviation. According to these findings for this kind of a system the analytical equations can be trusted and be used during the design.

- The system modeling is performed both with finite element method and experiments and the experimental system identification and some control algorithms are experimented on a real system. According to this evaluation, the result reached is that with the current instrumentation PI+FF+ZPETC controller is selected since this controller gives the desired response especially in sine tracking duty.

- Zero Phase Error Tracking Control with PI controller gives a performance quite close to PI+FF. PI+ZPETC controller could be used in such systems that the tracking capabilities is limited to a static positioning as this algorithm eliminates the modeling of a model based control (Bouc-Wen Model) which requires much calculation effort.

4.3 Recommentations for Future Work

Despite the results show the analytical model of the mechanism are accurate, some improvements can still be done on the models. For example the emprical formulations of flexure hinges can be revisited and improved on finite element method or using some other emprical formulations. The first future work aimed for this study is to integrate the designed mechanism to a real system which may be an alignment tool for a reflector feeder antenna system. In this manner a specific feeder reflector antenna system can be selected and a proper interface design can be added to mechanism and after that the performance of the mechanism can be observed. Moreover, a dynamic target tracking scenario can be selected and a proper interface of the mechanism can be designed and implemented. In addition, the control system of the mechanism can be improved. The friction during positioning can be investigated for different orientation of feeder. Actually, an interface for friction investigation is designed for the manufactured mechanism as in Figure 4.1 The friction can both be added to the model and experiments with a proper control system design.

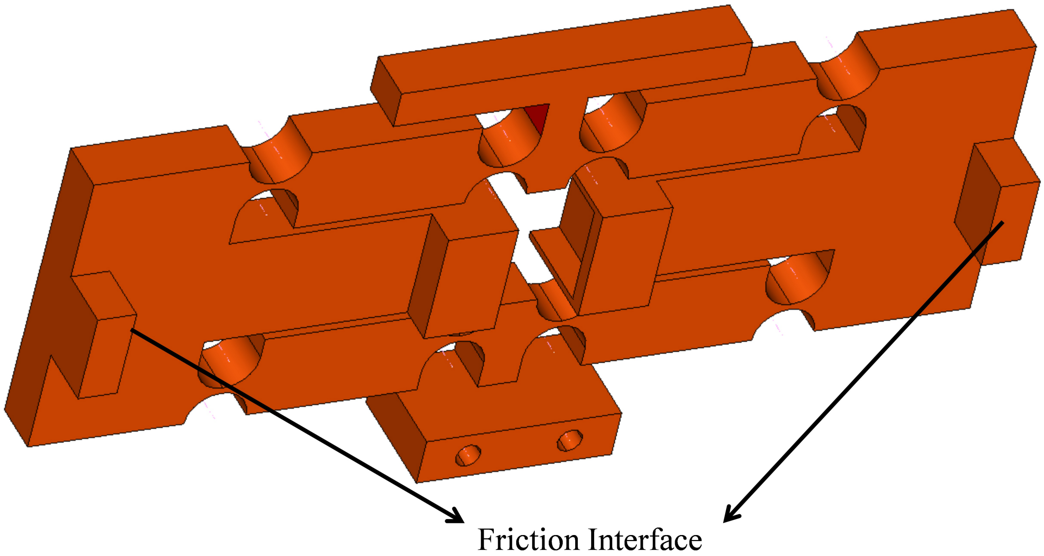

Figure 4.1: Friction Interface for the Designed Mechanism

Moreover in many precise positioning applications, a multi-axis stage configuration is needed and modeling a multi-axis mechanism using the methods displayed here can be a definite improvement to the system in future. The current design of the mechanism is hard to use in real life applications since the interface of the mechanism with the feeder is not designed and included to the system, a further work that includes the improving the structure to a more robust design which includes the mechanism, power amplifier and processor in one compact structure can be aimed to be completed.

REFERENCES

[1] http://www.physikinstrumente.com, Last visited on 2013.

[2] W.J. Kim. High precision magnetic leviation stage for photolithography. *Precision Engineering*, 22(2):66–77, 1998.

[3] S.C. Southward, C.J Radcliffe, and C.R. MacCluer. Robust nonlinear stick-slip friction compensation. *Dyn. Syst., Meas.*, 113:639–644, 1991.

[4] N. Lobontiu. *Compliant mechanisms: Design of Flexure Hinges*. CRC Press, 2003.

[5] L.L. Howell. *Compliant Mechanisms*. John Wiley & Sons, 2001.

[6] R.H Burns and F.R.E Crosley. Structural permutations of flexible link mechanisms. *ASME*, 66:5, 1996.

[7] T.E Shoup and C.W McLaran. On the use of the undulating elastica for the analysis of flexible link devices. *Journal of Engineering for Industry*, pages 263–267, 1971.

[8] A. Midha and L.L Howell. On the nomenclature and classification of compliant mechanisms: Abstraction of mechanisms and mechanism sysnthesis problem. *ASME*, pages 222–235, 1992.

[9] B. Salamon. Mechanical advantage aspects in compliant mechanisms design. Master's thesis, Purdue University, 1989.

[10] H. Navi. *Static and Dynamic Analysis of Compliant Mechanisms Containing Highly Flexibele Members*. PhD thesis, Purdue University, 1991.

[11] K. Y. Yong, T. Lu, and D. C. Handley. Review of circular flexure hinge equations and derivation of emprical formulations. *Science Direct*, 32:63–70, 2008.

[12] E. Garcia, Lobontiu, and Y. Nam. Design, modelling and initial experiments on microscale amplification device. *Journal of Intelligent Material Systems and Structures*, 16:10–39, 2005.

[13] M.N.M. Zubir and B. Shirinzadeh. Development of a high precision flexure-bases microgripper. *Precision Engineering*, 33:362–370, 2009.

[14] E. Tanık and V. Parlaktaş. A new type of compliant spatial four-bar (rssr) mechanism. *Mechanism and Machine Theory*, 46:593–606, 2011.

[15] L. Subaşı. Sysnthesis of compliant bistable four-link mechanisms for two positions. Master's thesis, Middle East Technical University, Mechanical Engineering Department, 2005.

[16] Y. Renyi. *Design and Modelling of Single Axis, Flexure Hinge Type, Micro Positioning Stages*. PhD thesis, University of Rhode Island, 1995.

[17] Y. Qing, J. Dong, and P.M. Ferreira. Design, analysis, fabrication and testing of a parallel-kinematic micropositioning xy stage. *International Journal of Machine Tools & Manufacture*, 47:946–961, 2007.

[18] R. C. Tjptoprodjo. On a finite element approach to modeling of piezoelectric element driven compliant mechanisms. Master's thesis, University of Saskatchewan, 2005.

[19] N. Jalili. *Piezoelectric-Based Vibration Control: From Macro to Micro/Nano Scale Systems*. Springer, 2009.

[20] Design and prototyping tools product catalog. Technical report, Piezo System Inc, 2002.

[21] *Publication and Proposed Revision of ANSI/IEEE Standard 176-1987 ANSI/IEEE Standard on Piezoelectricity*. IEEE Transactions on Ultrasonics, Ferroelectrics and Frequency Control.

[22] N. Christopher, B. Diann, B. Sivakumar, and M. Andrew. Piezoelectric actuation: State of the art. *Shock and Vibration Digest*, 33:269–280, 2001.

[23] J.L. Ha, Y.S. Kung, and R.F. Fung. Optimal design of a micro-positioning scott russell mechanism by taguchi method. *Sensors and Actuators*, 125:565–572, 2006.

[24] A. Doğan. *Flextensional "Moonie and Cymbal" Actuators*. PhD thesis, Pennsylvania University, 1999.

[25] Y. K. Yong, L. Tien-Fu, and D. C. Handley. Review of circular flexure hinge design equations and derivation of empirical equations. *, Precision Engineering*, 32:63–70, 2008.

[26] W. Schotborgh, F. Kokkeler, H. Trager, and F. van Houten. Dimensionless design graphs for flexure elements and a comparison between three flexure elements. *Precision Engineering*, 29:41–47, 2005.

[27] C.B. Ling. On the stresses in a notched strip. *ASME Applied Mechanics*, 74:141–144, 1952.

[28] C. B. Ling. On stress concentration factor in a notched strip. *ASME Applied Mechanics*, 90:833–835, 1990.

[29] M.M. John. Factors of stres concentration photoelastically determined structures. *ASME Applied Mechanics*, 57:A67, 1935.

[30] Low voltage co-fired multilayer stacks, rings and chips for actuation. Technical report, APC International USA, 2013.

[31] C. J. Roy and A. J. Kurdila. *Fundamentals of Structural Dynamics*. Wiley, 2006.

[32] S. N. Sivanandam and S. N. Deepa. *Introduction to Genetic Algorithms*. Springer, 2007.

[33] Ansys mechanical apdl coupled-field analysis guide. Technical report, ANSYS Inc., 2010.

[34] N. Clement and P. Francois. Identification methodoology of electrical equivalent circuit of the piezoelectric transformers by fem. 2010.

[35] S. Devasia, E. Eleftheriou, and S.O.R. Moheimani. A survey of control issues in nanopositioning. *IEEE Trans. Contr. Syst. Technology*, 15:802–823, 2007.

[36] M. A. Krasnoselskii and A. V. Pokrovskii. *Systems with Hysteresis*. Springer, 1989.

[37] S. Bashash and N. Jalili. Underlying memory-dominant nature of hysteresis in piezoelectric materials. *Journal of Applied Physics*, 100:103–141, 2006.

[38] L. Zhan-hui, Yun-xin Wu, and Deng Xi-shu. Modeling and compensating of piezoelectric actuator hysteresis in photolithography. *IEEE Proceedings of HDP07*, 2007.

[39] D. Hughes and T. W. John. Preisach modeling of piezoceramic and shape memory alloy hysteresis. *Smart Mater. Struct*, 6:287–300, 1997.

[40] D. Song. *Piezo Actuator Hybrid Modelling and Nonlinear Control for Active Error Compenastion in Diamond Turning*. PhD thesis, Rensselaer Polytechnic Institue, 1998.

[41] Y.K. Wen. Method of random vibration of hysteretic systems. *J. Eng Mech. ASCE*, 102:249–263, 1976.

[42] W. Low. Modelling of a three-layer piezoelectric bimorph beam with hysteresis. *IEEE Microelectromechanical Systems*, 4:230–237, 1995.

[43] R. Babuska and H. Verbruggen. Neuro-fuzzy methods for nonlinear system identification. *Annual. Rev. in cont.*, 27:73–85, 2003.

[44] M. Tomizuka. On the design of digital tracking controllers. *ASME J. of Dyn. Syst., Meas., and Control*, 115:412–418, 1993.

APPENDIX A

PROPERTIES OF PST150

PIEZOMECHANIK PSt150

Osi-multilayer ceramic

PROPERTIES OF PIEZOCERAMIC MATERIAL HS/HT

Property	Symbol & Unit	Value
DIELECTRICAL DATA		
Permittivity	$\varepsilon^T_{33} / \varepsilon_o$	5400
Dielectric Loss Factors	$tg\delta$ [10^{-4}]	200
ELECTROMECHANICAL DATA		
Coupling Factor	K_p	0.62
Coupling Factor	K_{31}	0.34
Coupling Factor	K_{33}	0.68
Piezoelectric Charge Constant	$-d_{31}$ [10^{-12} C/N]	290
Piezoelectric Charge Constant	d_{33} [10^{-12} C/N]	640
Piezoelectric Voltage Constant	$-g_{31}$ [10^3 Vm/N]	6
Piezoelectric Voltage Constant	g_{33} [10^3 Vm/N]	13.2
MECHANICAL DATA		
Elastic Compliance	$s^E{}_{11}$ [10^{-12} m^2/N]	14.8
Elastic Compliance	$s^E{}_{33}$ [10^{-12} m^2/N]	18.1
Young modulus	$Y^E{}_{33}$ [10^{10} N/m^2]	5.5
Young modulus	$Y^E{}_{11}$ [10^{10} N/m^2]	6.8

Radial Frequency Constant	$N^E{}_p$ [m/s]	2040
Thickness frequency Constant	$N^D{}_t$ [m/s]	1800
Transverse Frequency Constant	$N^E{}_1$ [m/s]	1400
Longitudal requency Constant	$N^D{}_3$ [m/s]	1370
Mechanical Quality Factor	Q_m	70
Density	ρ [10^3 kg/m^3]	8.00
THERMAL DATA		
Curie Temperature	T_c [^{o}C]	150

APPENDIX B

MATLAB SCRIPT PARSING ZPETC

```
function [Gzpet] = zpetc(transfer_func)

if length(transfer_func)>1,
    error('Too many inputs');
end
if isa(transfer_func {1},'tf')==0,
    error('Transfer function required');
end

clc;
Gclosed = transfer_func {1};

[num,den,Ts]=tfdata(Gclosed,'v');
if length(num)>length(den),
    error('Improper model');
end

[Z,P,K] = tf2zpk(num,den);%Poles and zeros of the system
j = 0;
k = 0;
Z_u = [];
Z_s = [];

for i=1:length(Z),
    if abs(Z(i)) >= 1,
        j = j+1
        Z_u(j) = Z(i)
    else
        k = k+1;
        Z_s(k) = Z(i)%The zeros that are inside the unity circle
    end
end

F1 = zpk(P, Z_s, K^-1, Ts);%form an inverse transfer function with stable
zeros
Bc_minus=zpk(Zs,[],K,Ts)
Bc_plus=zpk(Zu,[],1,Ts)
Ac=zpk(P,[],K,Ts)
Stable_inverse=Ac/Bc_plus;
F2temp = zpk(Zu, [], 1, Ts);%form a tf with unstable zeros
Gain = dcgain(F2temp);
Gain_comp_filter=K;
Gain_comp_filter=Gain_comp_filter^-1;
Gain_comp_filter=Gain_comp_filter^2
assignin('base','Gain_comp_filter',Gain_comp_filter)
assignin('base','Bc_minus',Bc_minus)
assignin('base','Bc_plus',Bc_plus)
assignin('base','Stable_inverse',Stable_inverse)
assignin('base','Ac',Ac)
```

```
Bc_minus=zpk(Zs,[],K,Ts)
Bc_plus=zpk(Zu,[],1,Ts)
Ac=zpk(P,[],K,Ts)
Stable_inverse=Ac/Bc_plus;
F2temp = zpk(Zu, [], 1, Ts);%form a tf with unstable zeros
Gain = dcgain(F2temp);%e
Gain_comp_filter=K;
Gain_comp_filter=Gain_comp_filter^-1;
Gain_comp_filter=Gain_comp_filter^2
assignin('base','Gain_comp_filter',Gain_comp_filter)
assignin('base','Bc_minus',Bc_minus)
assignin('base','Bc_plus',Bc_plus)
assignin('base','Stable_inverse',Stable_inverse)

assignin('base','Ac',Ac)
for p = 1:(j+1),
    N_u(j-p+2) = N(p);
end
Du = zeros(1,(j+1));
Du(1) = 1;

F2 = tf(Nu, Du, Ts);

F = F1*F2/Gain^2;
figure;
bode(Gclosed,'k:'); grid on;

legend('G_closed','G_controller','G_overall_sys');
[Az,Bz] = tfdata(F,'v');
nz = length(roots(Az));
np = length(roots(Bz));
d = nz - np
delay=zeros(1,d)
length(d)
Phase_Compansation_Filter=zpk(zeros(1,d),[],1,Ts);
Phase_comp_filt=Phase_Compansation_Filter*Bc_minus;
Overall_controller=sqrt(Gain_comp_filter)*(Phase_comp_filt)^-
d*Stable_inverse;
bode(Overall_controller);
bode(Overall_controller*Gclosed);
Gzpet=Overall_controller
```